95 GHz INSTRUMENTATION RADAR STUDY

Final Technical Report on
P.O. No. F13549

by

N. C. Currie, T. L. Lane, J. A. Scheer,
E. F. Knott, and D. S. Ladd

Prepared for

McDonnell Douglas Corporation
P. O. Box 516
St. Louis, Missouri 63166

Prepared by

Georgia Institute of Technology
Engineering Experiment Station
Atlanta, Georgia 30332

January 1982

TABLE OF CONTENTS

TABLE OF CONTENTS (Continued)

LIST OF FIGURES

LIST OF FIGURES (Continued)

LIST OF TABLES

SECTION 1
INTRODUCTION

This report summarizes the results of a study performed under Purchase Order Number F13549 to establish a preliminary design for a 95 GHz instrumentation radar sensor for use at the Grey Butte test range in California. This report summarizes the preliminary system tradeoff study, the final system concept and preliminay design, and estimated cost information. Also, the test range environmental impact on system performance and maintenance considerations for the proposed system are discussed.

1.1 CONTRACT TASK STATEMENT

Under the referenced Purchase Order the Georgia Institute of Technology Engineering Experiment Station was funded to perform three tasks. These included:

1. Conduct a study of the requirements for a 95 GHz instrumentation radar which includes block diagrams of the recommended approaches, determination of the expected performance of the recommended system (in particular to include the minimum detectable RCS), and a cost estimate for the system. Also, areas of technical or cost risk were to be identified.
2. Estimate the effects of the range environment including weather, multipath, and support structure effects and make recommendations concerning minimization of these effects.
3. Present the results of Tasks 1 and 2 in a briefing to the McDonnell Aircraft Company and in a final report.

After consultation with McDonnell personnel, Task 1 was broken into two subtasks: Subtask A involved a preliminary design, cost estimation, and performance evaluation for three candidate systems involving different technologies. Subtask B consisted of a detailed design of the specified candidate system chosen by McDonnell. The results of Task 1-A are summarized in Section 1.2, and the final design resulting from Task 1-B is given in Sections 3 through 6.

The environmental and range geometry effects on the system (Task 2) are summarized in Section 2. The briefing called for in Task 3 was presented to McDonnell personnel on 24 November 1981, and this report fulfills the remaining requirement on Task 3.

1.2 PRELIMINARY DESIGN RESULTS

Preliminary designs were established for three candidate systems utilizing different technologies so that a rough performance/cost tradeoff analysis could be made in time to allow a more detailed design of the designated system. The three candidate systems involved the use of an Extended Interaction Oscillator (EIO) transmitter with an incoherent receiver, a solid state Impatt amplifier chain with a coherent receiver, and an Extended Interaction Amplifier (EIA) driven by a solid state low power amplifier chain with a coherent receiver. Table 1 summarizes the salient characteristics of each system. The EIO with the incoherent receiver provides high power, but low integration gain. The solid state system provides high integration gain, but low peak power. And the EIA system provides high power and high integration gain, but is a more complex system. If the range parameters given in Table 2 and the radar parameters given by Table 3 are assumed, then the values for the minimum detectable radar cross section (RCS) can be calculated from the radar range equation.

$$\sigma_{min} = \frac{(S/N)\ (4\ \pi)^3\ R^4\ Kt\ B_n\ F_n\ L_s}{P_t\ G_t\ G_r\ \lambda^2\ N} \qquad (1)$$

where:

σ_{min} = Minimum Detectable RCS
S/N = Signal-to-Noise Ratio (= 1)
R = Slant Range (= 1170 m)
K = Boltzmann's Constant
t = Receiver Temperature
B_n = Receiver Bandwidth
F_n = Receiver Noise Figure
P_t = Transmitter Power
G_t = Transmitter Antenna Gain
G_r = Receiver Antenna Gain
λ = Wavelength
L_s = Total Losses
N = Integration Gain

Table 4 summarizes the resulting calculated minimum detectable radar cross-section for each system as well as the estimated cost for each system based on data presented in Reference 1.

The results of the preliminary design can be summarized as follows: 1) The sensitivities of the EIO and solid state systems are similar, but the sensitivity of the EIA system is significantly better (approximately 17 dB better). 2) The estimated cost of the EIA system is 25% greater than the EIO or solid state systems. 3) In terms of complexity and, therefore, overall reliability, the EIO, solid state, and EIA systems range in descending order.

Based on these preliminary results, McDonnell chose to pursue a final design for the Extended Interaction Amplifer - based system. This design is discussed in Sections 3 through 6.

TABLE 1. PRIMARY CHARACTERISTICS OF EACH CANDIDATE SYSTEM

	System Characteristics		
Parameter	EIO	Solid State	EIA
Peak Transmitter Power	1 kW (2 kW)[1]	10 W	1 kW (2 kW)
Maximum PRF	25 kHz	60 kHz (100 kHz)	25 kHz
Integration Type	Incoherent	Coherent	Coherent
Maximum Integration Gain[2]	17 dB	38 dB (40 dB)	34 dB

1 ( ) Indicates typical but not guaranteed Values

2 Assumes no integration losses

TABLE 2. RADAR PARAMETERS DETERMINED BY TEST RANGE GEOMETRY

Parameter	Value	Comments
Range	1170 m	Longest Measurement Distance
Target Dimensions	20 m Long x 5 m High	Determines Minimum Beamwidth, Pulse Length
Minimum Bandwidth For 1^{o} Taper on Target	2^{o}	Cover Target Length Cross Range
	0.5^{o}	Cover Target Height
Minimum Pulse Length	200 ns	Since Target Length is 20 m, assumes "Pulse Fill" on Target
Atmospheric Loss	0.5 dB	Estimated Round Trip Loss
Integration Time	0.1 s	Range Data Rate

TABLE 3. ASSUMED RADAR PARAMETERS FOR PRELIMINARY SENSITIVITY CALCULATIONS

Parameter	System Classification		
	EIO	Solid State	EIA
Transmitted Power	1 kW (2 kW)[1]	10 W	1 KW (2 kW)
Pulse Length	200 ns	200 ns	200 ns
Transmitting antenna Gain[2]	44.5 dB	44.5 dB	44.5 dB
Receiving Antenna Gain[2]	44.5 dB	44.5 dB	44.5 dB
Wavelength	3.16 mm	3.16 mm	3.16 mm
Receiver Bandwidth	5 MHz	5 MHz	5 MHz
Kt ($t = 273^{o}$)	-204 dB	-204 dB	-204 dB
Receiver Noise Figure	8 dB	8 dB	8 dB
Signal-to-Noise Ratio	0 dB	0 dB	0 dB
Range	1170 m	1170 m	1170 dB
Total Losses[3]	10 dB	10 dB	10 dB
Integration Gain[4]	17 dB	38 dB (40 dB)	34 dB

1. Numbers in parenthesis ( ) indicate expected values.
2. Assumes 2^{o} x $1/2^{o}$ fan beam which provides 1 dB taper across target at 1170 meters.
3. 3 dB Tx loss + 6 dB Rx loss + 1 dB atmospheric loss.
4. Assumes 2500 pulses integrated for the EIO and EIA systems, and 6000 (10,000) pulses integratred for the solid state system.

TABLE 4. ESTIMATED RADAR SENSITIVITY VERSUS COST

Parameter	System Characteristics		
	EIO	Solid State	EIA
Guaranteed Performance[1]	-50 dBsm	-51 dBsm	-67 dBsm
Probable Performance[2]	-53 dBsm	-53 dBsm	-70 dBsm
Preliminary Estimated Cost	$554,000	$576,000	$697,000

1. Assumes 1 kW transmitter power and 25 kHz PRF for EIO and EIA systems, and 10 W transmitted power and 60 kHz PRF for solid state systems.

2. Assumes 2 kW transmitter power and 25 kHz PRF for EIO and EIA systems, and 10 W transmitter power and 100 kHz PRF for solid state systems.

3. Does not have "inflation factor" built into manpower estimate.

SECTION 2
RANGE EFFECT ON SYSTEM PERFORMANCE

The physical constraints put on the system performance by the test range environment are discussed in this section. These effects include the range which affects the sensitivity, the maximum target size which affects the antenna dimensions and thus the sensitivity, ground plane effects including possible sensitivity enhancement as well as calibration errors, target support structure limitations, and atmospheric effects.

2.1 ANTENNA SELECTION

To achieve the desired system sensitivity, designers often have to select large antennas to compensate for sensitivity limitations elsewhere in the system. Unfortunately, this cannot be done indiscriminately because the accuracy of the data collected with the radar may be degraded. A large antenna with a narrow beam is desired to concentrate the radiated power in the vicinity of the target and to reduce background clutter. But if the incident beam is too narrow, there will be a significant -- and perhaps unacceptable -- taper in the amplitude distribution from one side of the target to the other.

The effect of antenna size can be estimated by assuming that the reflector is illuminated by a signal having a cosine distribution in field strength from one side of the aperture to the other, e.g., the field strength is maximum at the center and tapers to zero at the rim. The field pattern due to such a distribution is[2]

$$f(w) = \frac{\cos\ (\pi w/2)}{1 - w^2} \qquad (2)$$

where: $w = (1/\pi)\, kd \sin\ \phi$,

$k = 2\pi/\lambda$, the free space wave number,

d = antenna diameter

ϕ = off-boresight angle

---

[2]John D. Kraus, Antennas, McGraw-Hill, 1950, p. 350

The boresight gain of the antenna is

$$G = \eta \left(\frac{1}{2} kd\right)^2 \tag{3}$$

where η is the efficiency, typically about 50% at millimeter wavelengths for conventional dishes and feeds.

For a given range R and transverse target length L, the angle subtended at the radar by the ends (or sides) of the target is approximately given by

$$\sin \phi = L/2R \tag{4}$$

To establish the maximum allowable size of the antenna for this combination of range and target size, we need to specify an allowable amplitude taper from the center of the target to its extremes. Consequently, given a value for $f(\phi)$, we need to determine the w in Equation (2) that produces that level.

This generates a transcendental equation in w,

$$0 = f - \frac{\cos(\pi w/2)}{1 - w^2} \tag{5}$$

which can be solved using the Runge-Kutta method of successive approximations. Specifically, we form a function g,

$$g = f - \frac{\cos(\pi w/2)}{1 - w^2}$$

and its derivative

$$\frac{dg}{dw} = \frac{\pi/2\,(1 - w^2)\sin(\pi w/2) - 2w\cos(\pi w/2)}{(1 - w^2)^2} \tag{6}$$

The method requires that a reasonably close trial value be assumed for w and that a correction

$$\Delta = g \Big/ \frac{dg}{dw} \tag{7}$$

be formed and subtracted from w. The new value of w may itself be corrected by repeating the procedure until the correction becomes acceptably small. Table 5 lists the arguments w for several values of f(w).

TABLE 5. SOME SOLUTIONS OF EQUATION (5).

20 log |f|	w
-0.10	0.222
-0.25	0.350
-0.50	0.494
-1.00	0.696
-2.00	0.977
-3.00	1.187
-4.00	1.359
-5.00	1.507

We now observe that

$$w = \frac{1}{\pi} kd \sin \phi \approx \frac{dL}{\lambda R} \tag{8}$$

which can be solved for d,

$$d = w \lambda R/L \tag{9}$$

Thus, given an amplitude taper, the wavelength, the range, and the target size, we may determine the maximum allowable antenna size that assures the amplitude taper will not exceed the specified value.

The results are plotted in Figure 1 for several amplitude tapers. The plot and Equation (8) show that smaller antennas are needed for larger targets, and the more uniform the amplitude distribution (the smaller the taper), the smaller the antenna must be. Assuming that targets no larger than 25 feet will be measured, Figure 1 suggests that an antenna no larger than 5.7 inches in diameter may be used for a 1-dB taper or less at 1650 feet. This amount of taper is acceptable for all but the most exacting measurements. If the taper tolerance is relaxed to 2 dB, then the antenna diameter may be as much as 8 inches, but this should be avoided, if possible, in the interest of maintaining data accuracy.

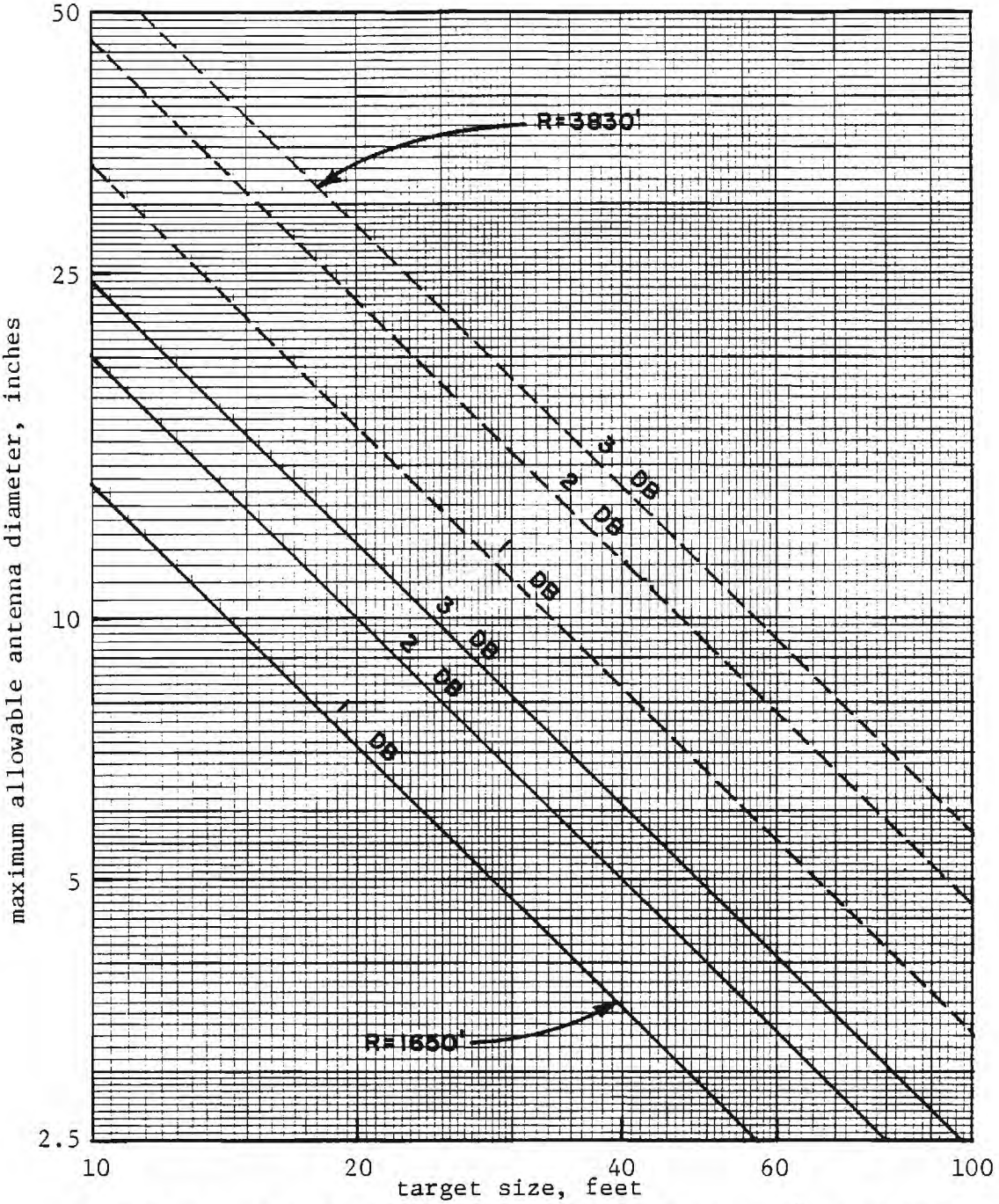

Figure 1. Maximum allowable antenna size to hold amplitude taper at or less than the indicated values at 95 GHz.

Similarly, the boresight gain may be calculated if Equation (8) is solved for kd and the result is used in Equation (3). Then we have

$$G = \eta \, (\pi w R/L)^2 \tag{10}$$

and this is plotted in Figure 2 for an efficiency of 50%. Since a target of fixed length subtends a smaller angle at greater range, higher antenna gains are allowable at the 3830-foot range than at the 1650-foot range. Figure 2 shows that, for a 1 dB taper over a 25-foot target, the maximum antenna gain is 47.5 dB at the greater range, but only 40 dB at the near range. Allowing a degradation to a 2-dB taper increases these values 3 dB (to 50.5 and 43 dB, respectively). The gain can be further increased by 5 dB if a 3:1 fan beam is used, as discussed later. This reduces the ground illumination and concentrates more energy on the target.

It can be seen that optimum selection of antenna gain depends on the illumination taper one is prepared to accept and on the range to the target. If it is not practical to switch from one antenna size to another, more accurate data requirements would indicate an antenna selection based on the closer range (1650 feet). If sensitivity requirements are more important than accuracy, the selection would be based on sensitivity alone. In either event, however, the use of a fan beam is recommended, with the narrower beam dimension being in the vertical plane.

In addition to measurement errors due to the amplitude taper over the transverse target dimensions, errors will be caused by phase deviations. The classic far field requirement

$$R = 2L^2/\lambda \tag{11}$$

is the result of demanding that the phase deviation over a transverse target dimension (due to spherical incident phase fronts) not exceed 22.5 degrees. At 95 GHz it is impractical to place all but the smallest target in the near field.

This is demonstrated in Figure 3, where the far field distance is plotted against the target size for a frequency of 95 GHz. This figure shows that a 9-foot target would have to be measured at a range of 3 miles, a 12-foot target at 4 miles and a 15-foot target at 8 miles. According to this criterion, targets would have to be smaller than 4.5 feet to be measured at the 3830-foot range and smaller than 3 feet for the 1650-foot range. Obviously, the far field range will scarcely ever be met for most targets of interest.

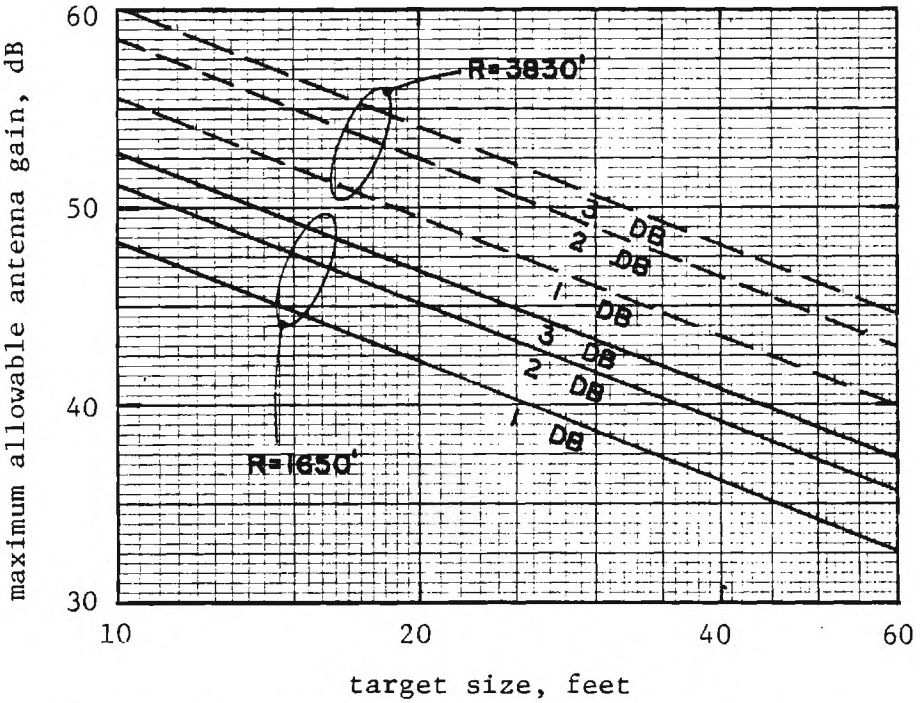

Figure 2. Maximum allowable antenna gain to hold amplitude taper at or less than the indicated values at 95 GHz. Antenna efficiency of 50% has been assumed. For a 3:1 fan beam, these lines should be displaced upward on the chart by 5 dB.

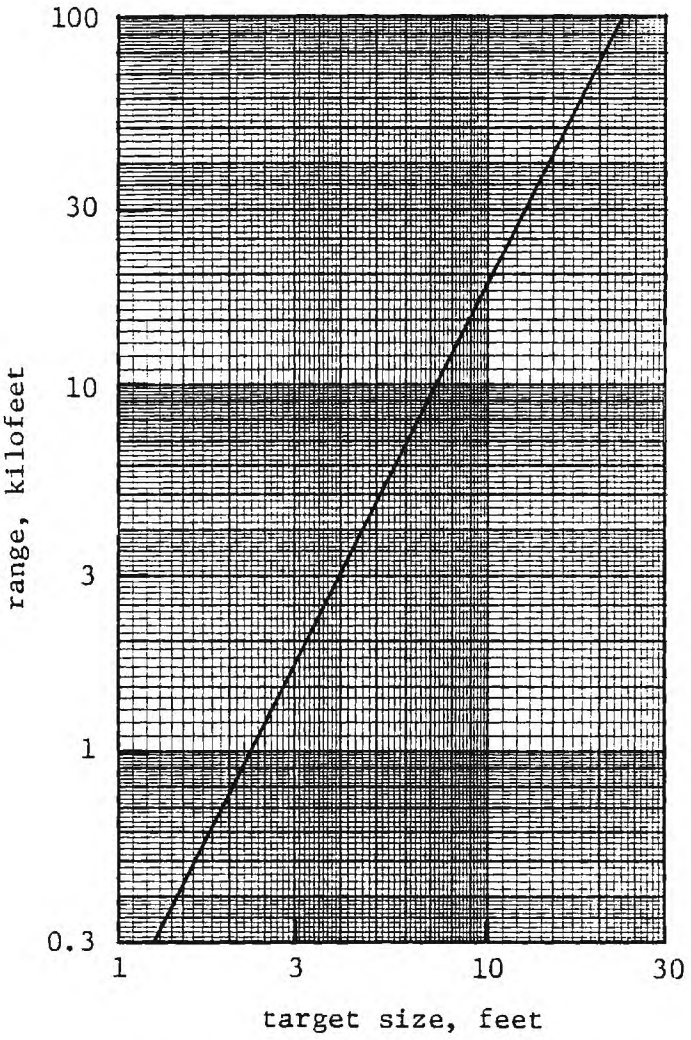

Figure 3. Far field distance at 95 GHz.

However, one can argue that most targets of interest will not have a straight edge or surface sufficiently smooth to require flat phase fronts. The mean amplitude of the measured RCS pattern will be practically identical to that measured in the true far field, although the peaks and nulls of the pattern may be shifted slightly. At mm wavelengths the lobe structure will be so fine that the locations of peaks and nulls will lose their significance anyway.

This is not true of a straight smooth scatterer like a cylinder. The first symptom of near field effects is the lack of depth in the first few nulls near the broadside aspect angle. As the target is brought closer in the near field, the sidelobes begin to increase slightly in amplitude. At very close ranges, the nulls are only a few dB below their adjacent peaks, and the broadside return is reduced in amplitude. These features would not be noticeable for a complicated target, because a complicated target would not have a single straight element running from one end to the other. Thus, near field effects can be tolerated for complex targets, whereas the errors could be severe for very simple targets.

2.2 RANGE EFFECTS

It is doubtful if the ground plane effect can be exploited at millimeter wavelengths. There are two reasons for this: 1) the ground, even asphalt, is likely to be rough enough to spoil the good forward reflection at the specular point, and 2) the gain of the antenna will have to be high enough (i.e., the beam narrow enough) that the specular point probably will not be adequately illuminated by the antenna beam. To study the effect of surface roughness, we will use Barton's model for the diffuse field at the target due to a rough ground plane between the target and the illuminating antenna.[3]

Barton assumes that the rough surface between the antenna and the target can be represented as a "glistening" surface consisting of a collection of flat facets, each tilted away from the horizontal by some angle β. He argues that the facet tilt is uniformly distributed up to a maximum angle β_o for a rough surface. Thus the diffuse power arises from a surface bounded by facets whose slopes are less than β_o.

Unlike the contribution due to the specular reflection off the ground surface, the diffuse contribution arises from ground elements ranging from near the antenna to near the target. The diffuse multipath geometry sketched in Figure 4a shows a ground element located a distance x_1 from the radar; the incident ray hits the ground at an angle ψ_1 while the diffused ray subtends an angle ψ_2. For specular reflections these

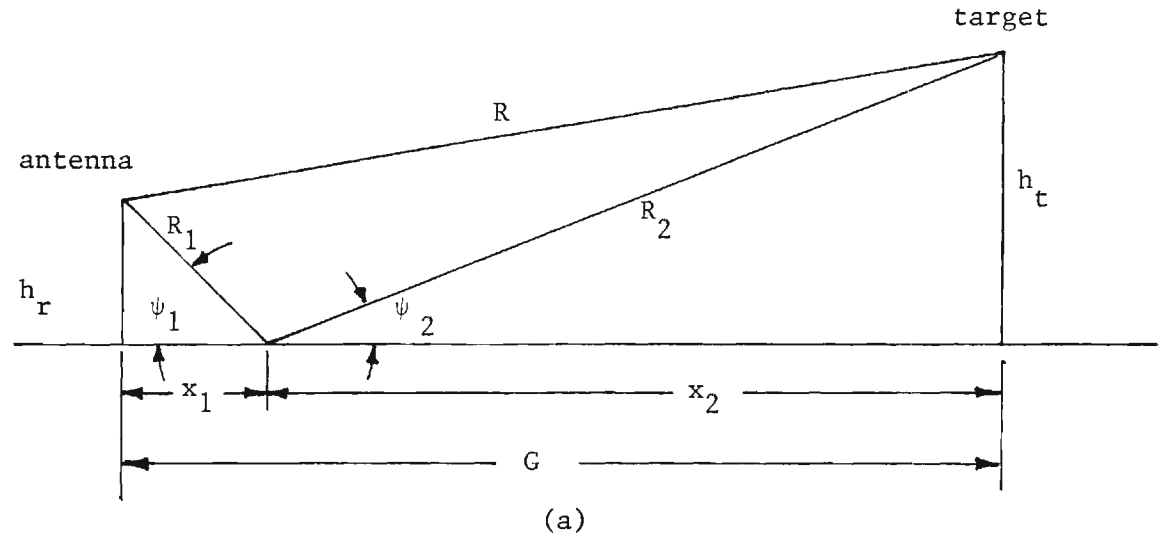

(a)

Geometry for Barton's diffuse multipath model

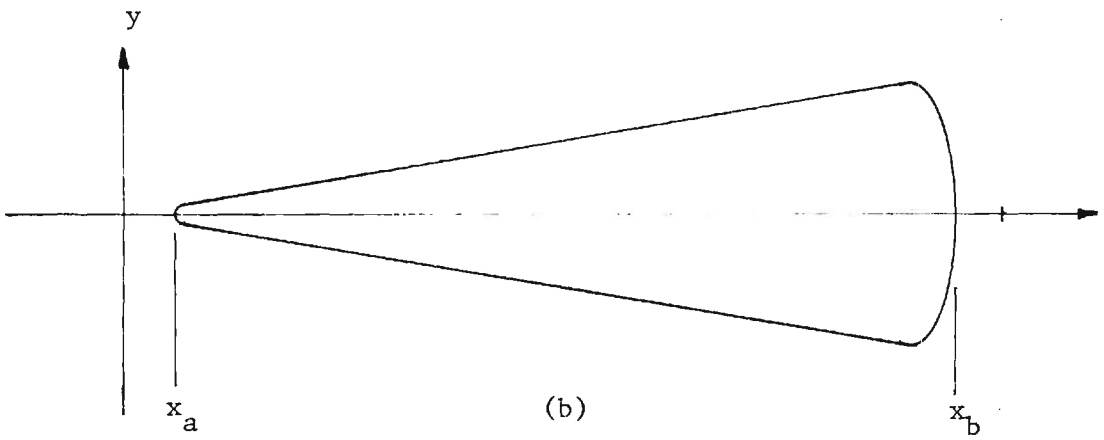

(b)

The glistening surface

Figure 4. Geometry for considering range effects.

angles are equal, but not for the diffuse contributions. The slant range to the target is R and the horizontal range (as measured along the ground) is G.

Figure 4b shows the glistening surface. The glistening surface is only a few feet wide, hence the y-coordinate in this figure is shown greatly expanded. The glistening surface does not extend quite to the radar nor quite to the target; its limits are $x = x_a$, x_b as shown in the diagram. Barton gives the coordinates of the glistening surface as

$$y = \pm \frac{\frac{h_r + h_t}{x_1 + x_2}}{\frac{1}{x_1} + \frac{1}{x_2}} \left\{ \beta_o^2 - \frac{1}{4} \left(\frac{h_r}{x_1} - \frac{h_t}{x_2} \right)^2 \right\}^{1/2} \tag{12}$$

where h_r and h_t are the radar and target heights, respectively, above the ground plane and x_1 and x_2 are as shown in Figure 4a.

For the low angle case, in which $h_r << R$, $h_t << R$, Barton expresses the diffuse multipath contribution to the incident power on the target, relative to the direct illumination, as

$$\rho_d^2 \simeq \frac{1}{2 \pi \beta_o^2} \int_{x_a}^{x_b} \frac{R^2 y \, dx}{(R-x)^2 x^2} \tag{13}$$

where the limits of integration are

$$x_a = h_r / 2\beta_o, \quad x_b = R - h_r / 2 \beta. \tag{14}$$

This expression does not include the antenna power pattern because Barton has assumed the pattern to be broad enough, and the angles small enough, that the antenna pattern has a small effect. To account for the intensity of the ground illumination, we will multiply the integrand of Equation (13) by the square of Equation (2), which is the antenna power pattern.

To account for the effect of some small bumps in the ground masking others from direct illumination by the antenna, Barton introduces a roughness factor F_d^2,

$$F_d^2 = \left\{ (1 - \rho_{s1}^2)\ (1 - \rho_{s2}^2) \right\}^{1/2} \tag{15}$$

where

$$\rho_{s1} = \exp \left\{ -2\ (k\ \sigma_h \sin \psi_1)^2 \right\} \tag{16}$$

$$\rho_{s2} = \exp \left\{ -2\ (k\ \sigma_h \sin \psi_2)^2 \right\} \tag{17}$$

σ_h = RMS surface height.

Thus the integral in Equation (13) can be evaluated by incorporating Equations (2) and (15) as multipliers of the integrand.

However, the pattern given by Equation (2) has many lobes and nulls, especially for angles more than 2 or 3 degrees off the antenna boresight. This is due to the rapid variations of the cosine function in the numerator. To simplify the integration, we will therefore set the numerator identically to one. This represents a "worst case" situation, because the actual pattern will always be less than or equal to the artificial case when $\cos(\lambda w/2) = 1$. In effect, we will use the envelope of the antenna power pattern.

Finally, we anticipate that the illuminating antenna will be mounted at approximately the same height as the target, since we are trying to defeat the ground plane to begin with. This sets $h_r = h_t$, whence Equation (12) is simply

$$y = \pm \beta_o$$

The resulting integral to be evaluated is

$$\rho_d^2 \simeq \frac{h_t}{2\pi\ \beta_o} \int_{x_a}^{x_b} \frac{R^2\ dx}{(R-x)^2\ x^2 \left[1 - \left(\frac{1}{\pi}\ kd \sin \psi_1 \right)^2 \right]^2} \tag{18}$$

where d is the diameter of the illuminating antenna in the vertical plane.*

*This automatically accounts for fan beams because it is only the pattern in the vertical plane that influences the diffuse multipath.

Equation (18) is easier to evaluate numerically than it is analytically. For this purpose, the integral was evaluated as a series of contributions from 20 strips of equal length Δx lying between $x = x_a, x_b$. The relative contribution as a function of x is shown in Figure 5 for an RMS surface roughness of one wavelength at 95 GHz for a fan beam generated by a 10 x 30 inch antenna aperture, with the 30-inch dimension being in the vertical plane. The maximum tilt β_o was assumed to be 0.1 radian, the range was assumed to be 1650 feet and the antenna (target) height was assumed to be 15 feet.

The incremental contribution from the ground near the antenna is of the order of 10 dB less than that near the target, and this is a consequence of the roll-off in the antenna power pattern at angles where the ground near the antenna is illuminated. The entire curve would be raised some 5 dB for a 10 x 10 inch aperture, and that portion near the antenna would be raised slightly more than 5 dB.

The net contribution to the diffuse multipath is, in effect, the area under the curve of Figure 5. Thus the integrated result would probably be of the order of -60 dB. In fact, when the integration is performed, the result is -62.5 dB, as may be read from the lower curve (for a 10 x 30 inch aperture) of Figure 6 for $\sigma_h = \lambda$. The diffuse multipath field increases as the ground plane becomes rougher. For a surface roughness of 3λ, for example, the contribution is -54 dB, an increase of 8.5 dB.

The upper curve of Figure 6 shows the estimated diffuse multipath contribution for a 10 x 10 inch antenna, and is approximately 21 dB higher. For this size antenna and a very rough surface ($\sigma_h = 10\lambda$), the diffuse contribution due to the ground is only 24 dB below the incident power.

The specular contribution, had there been a perfectly smooth ground plane at the specular point, would have been -17.6 dB and -37.6 dB for the 10 x 10 and 10 x 30 inch apertures, respectively. Even though the actual specular reflection would be less than this, the 20 dB improvement due to the bigger aperture is significant. Thus, it appears that the additional sensitivity and reduced multipath available by use of a fan beam might be worth the additional complication of designing and building such an antenna.

As far as the roughness of the ground is concerned, a one-wavelength RMS surface height is only 1/8 inch at 95 GHz, and the ground (or pavement) is almost assuredly at least that rough, but probably not as rough as 10 wavelengths. Since the diffuse multipath will probably not exceed -25 or -30 dB, there is no need to provide special ground treatments (i.e., roughening or smoothing). Moreover, the use of a fan beam will reduce the specular contribution of the ground to a level not much above that value. A

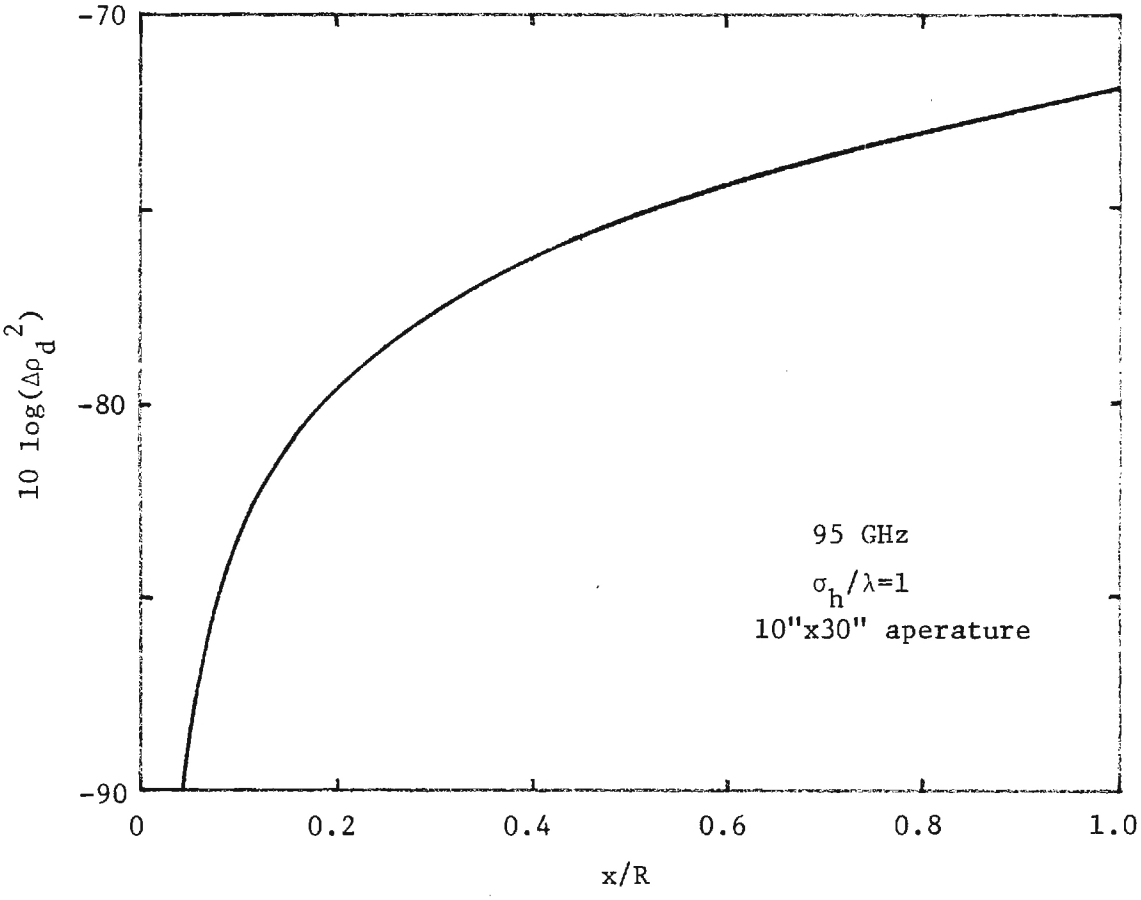

Figure 5. Incremental contribution to the diffuse multipath as a function of location downrange.

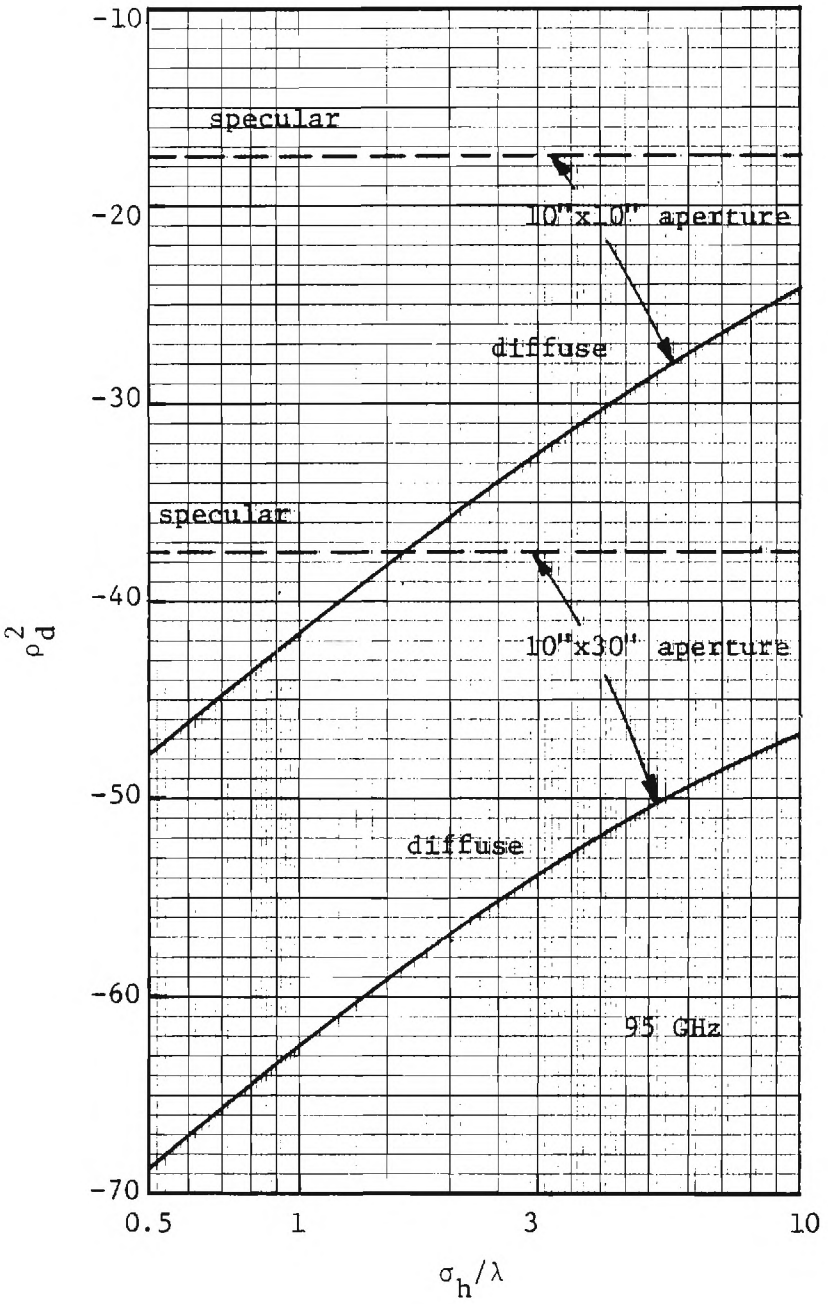

Figure 6. Influence of surface roughness on the diffuse multipath field. Specular contributions shown for comparison.

10 x 30 inch aperture is therefore recommended for the antenna, since this will increase the energy concentration on the target, minimize the specular reflection from the ground, and minimize the diffuse multipath illumination of the target.

2.3 THE GROUND PLANE EFFECT

If we attempt to preserve the ground plane effect rather than to destroy it, the antenna radiation pattern must be broad enough to illuminate the specular point and the first few Fresnel zones in its vicinity. Assuming for the moment that the antenna pattern has the required broadness in coverage, we need to establish the antenna height for a given target height. The net incident field at the target is the phasor sum of the direct illumination and the illumination via a reflection from the ground plane,

$$E_i = e^{ikR} + \rho e^{ik(R_1 + R_2)} \tag{19}$$

where R_1 is the distance from the antenna to the specular point, R_2 is the distance from the specular point to the target, and ρ is the voltage reflection coefficient of the ground plane surface.

For most ground planes, $\rho \simeq -1$, and even for imperfectly conducting ground planes, the phase angle of the reflection coefficient is close to 180 degrees, even if the amplitude is not 100%. The major effect of imperfect conduction at low angles of incidence is a reduction of the amplitude of the lobes generated by the interference pattern of the two arriving wavefronts; the locations of the lobes are relatively unaffected.

If the heights h_r and h_t are significantly less than the range R, the path length difference δ is

$$\delta = R - R_1 - R_2 \simeq 2h_r h_t / G \tag{20}$$

where G is the horizontal range to the target. The incident power distribution is approximately

$$|E_i|^2 \simeq 2\,(1 - \cos k\delta) \tag{21}$$

and takes on a maximum value of 4 when the electrical path length difference is an odd multiple of π radians. On the return trip the ground plane enhances the received signal, also by a factor of 4, thereby accounting for the 12 dB ($10 \log_{10} 16$) enhancement attributed to ground planes. But the target must be placed so as to be in one of the lobes where the direct and indirect incident waves reinforce each other

By imposing the requirement that $k\delta = m$, where m is an odd integer, we find that the target and antenna heights must be related by

$$h_r h_t = m \lambda G/4 \tag{22}$$

One customarily selects the first lobe (m = 1) to place the target in, because this yields the minimum illumination taper across the vertical target dimensions. (It is not an absolute requirement, however.) Thus, we obtain the classic antenna height/target height requirement,

$$h_r h_t = \lambda G/4 \tag{23}$$

Since the target height is presumably fixed at about 15 feet for a range of 1650 feet, the antenna height is very low, i.e., about 3.42 inches for a frequency of 95 GHz. This is less than the radius of even a 10-inch diameter antenna, and it is questionable that the full ground plane effects can be obtained when the lower rim of the antenna is placed below the ground, as is often done at RATSCAT, in an attempt to satisfy Equation (23). Nevertheless, let us assume that a small enough antenna can be used to do so, and that its radiation pattern is unaffected by the presence of the ground plane.

The angle ψ_1 is

$$\psi_1 = \arctan \frac{h_r + h_t}{G} \tag{24}$$

and is about 0.53 degree for the assumed geometry. The distance x_1 (in front of the antenna) to the specular point is

$$x_1 = G h_r/(h_r + h_t) \tag{25}$$

and amounts to about 30 feet. In general, it is not sufficient that the ground in the vicinity of the specular point be perfectly smooth and reflecting; the first few Fresnel zones must also be included in the smooth ground plane. "Fresnel zones" in this context are those regions on the ground where the path length difference varies by less than an integral number of radians.

Surfaces of constant path length difference are ellipsoids of revolution about the line connecting the target and the antenna. The intersection of these ellipsoids with the ground surface is a family of ellipsoids. Because of the small antenna and target heights compared to the range, these ellipses are extremely elongated, as may be seen from Table 6. The fourth Fresnel zone is more than 400 feet long, but less than 5 feet wide, for example. If we assume that the fourth zone must be included in any treatment of the ground plane to assure a good reflection, then the treatment must extend as far as 419 feet in front of the antenna. This is necessary to improve the specular reflection from the ground.

Another requirement is to minimize the diffuse reflection, implying that the ground treatment should probably be wide enough to include the main beam and the first few sidelobes of the antenna pattern where the energy strikes the ground. Assuming as a worst case that the antenna gain has been chosen to provide no more than a 2 dB taper across the maximum lateral target dimension, the antenna pattern is given by Equation (2) for a diameter of about 8 inches.

We seek the lateral distance y at a distance x = 419 feet where a given portion of the antenna pattern intercepts the ground. As viewed from the antenna, this point occurs at some depression angle ε and some azimuth angle α. Both angles will be small and the off-boresight angle is approximately

$$\phi \simeq (\alpha^2 + \varepsilon^2)^{1/2} \tag{26}$$

The antenna height is much smaller than the downrange distance x, and the lateral distance to the point will also be small compared to x. Hence,

TABLE 6. THE FIRST FOUR FRESNEL ZONES*

Path Length Difference, Wavelengths	x_a, ft	x_b, ft	Length, ft	Width, ft
0.5	30.74	30.74	0	0 (specular point)
1.0	5.35	164.36	159.01	1.53
1.5	3.15	260.99	257.84	2.56
2.0	2.24	345.03	342.79	3.40
2.5	1.73	419.22	417.19	4.40

*Range = 1650 feet
antenna height = 3.42 inches
target height = 15 feet
frequency = 95 GHz

$$\epsilon \simeq h_r/x \tag{27}$$

$$\alpha \simeq y/x \tag{28}$$

The nulls of the antenna pattern occur at odd integral values of $w = m$, $m \neq 1$, and for small off-boresight angles,

$$w \simeq kd\phi/\pi \tag{29}$$

We may now solve Equation (29) for ϕ and Equation (26) for α. When the substitutions indicated in Equations (27) and (28) are made, the lateral location of the point is

$$y \simeq \left[\left(\frac{m \lambda x}{2d} \right)^2 - h_r^2 \right]^{1/2} \tag{30}$$

The second term in the radical of Equation (30) is much smaller than the first and may be neglected. The width of the required ground plane treatment will be twice the value of Equation (30),

$$\text{width} \simeq m \lambda x/d \tag{31}$$

This allows us to estimate the width of the ground plane treatment depending upon how much of the antenna pattern it is necessary to include. Table 7 lists some typical results for the fourth Fresnel zone.

If it is necessary to include only the main lobe, then the width of the ground plane need be only about 20 feet, whereas a 45-foot wide ground plane would be required if the full second sidelobe were to be included. The actual selection depends on the roughness of the ground beyond the width indicated in Table 7; if the ground is smooth, a 20-foot width may be adequate.

TABLE 7. GROUND PLANE WIDTH*

Pattern Features Included	m	Width, feet
main lobe	3	19.5
main lobe plus first sidelobe	5	32.5
main lobe plus first two sidelobes	7	45.6

*for fourth Fresnel zone, x = 419 feet,
antenna diameter d = 8 inches

The question remains, how smooth must the ground be? The effective voltage reflection coefficient of a rough surface is

$$\rho = \Gamma \exp (-2k \sigma_h \sin \psi)^2 \tag{32}$$

where Γ is the classic Fresnel reflection coefficient associated with a dielectric interface[4]. The Fresnel reflection coefficient depends on the dielectric constant of the ground plane material and upon the angle of incidence, but we know of no measurements of the properties of soil or asphalt at these high frequencies. Nevertheless, if the dielectric constant ε_r were known, the Fresnel coefficients would be

$$\Gamma_h = \frac{(\varepsilon_r - \cos^2\psi)^{1/2} - \varepsilon_r \sin\psi}{(\varepsilon_r - \cos^2\psi)^{1/2} + \varepsilon_r \sin\psi} \tag{33}$$

$$\Gamma_e = \frac{\sin\psi - (\varepsilon_r - \cos^2\psi)^{1/2}}{\sin\psi + (\varepsilon_r - \cos^2\psi)^{1/2}} \tag{34}$$

for the incident magnetic and electric fields parallel to the ground surface, respectively. It should be noted that ε_r is complex in general, and that the imaginary component increases with moisture content.

At low grazing angles, $\sin\psi << 1$ and $\cos\psi \simeq 1$, hence we can approximate Equations (33) and (34) by

$$\Gamma_h \simeq 1 - \frac{1}{4}\frac{\varepsilon_r^2 \sin^2\psi}{\varepsilon_r - \cos^2\psi} \quad \text{(vertical polarization)} \tag{35}$$

$$\Gamma_h \simeq -1 + \frac{1}{4}\frac{\sin^2\psi}{\varepsilon_r - \cos^2\psi} \quad \text{(horizontal polarization)} \tag{36}$$

The amplitudes of these reflection coefficients are sensibly unity for low grazing angles, but one is positive and the other is negative. Recall in the derivation of Equation (22) that the effective reflection coefficient was assumed to be $\rho = -1$; therefore if the actual reflection coefficient is positive, the target will inadvertently be placed in a null of the interference pattern instead of at a peak. The lobe position can be restored to the appropriate target height, of course, by an adjustment of the antenna height, but if the

soil properties are unknown, this adjustment may have to be by trial and error. In an extreme case, it could be time consuming to find the proper antenna height.

This question aside, let us return to Equation (21), which was derived from Equation (19). We may allow ρ to have a phase angle Δ that depends on the effective dielectric constant of the ground plane, and this can be expressed as

$$\rho = |\rho| e^{i\Delta} \tag{37}$$

Thus, a more general form of Equation (19) is

$$|E_i|^2 = 1 + 2|\rho|\cos(k\delta + \Delta) + |\rho|^2 \tag{38}$$

where δ is the path length difference between the direct and reflected rays from the specular point. Even though the peaks of Equation (38) may occur at vertical positions different from those predicted by Equation (22), the maximum value at a peak is

$$|E_i|^2_{max} = (1 + |\rho|)^2 \tag{39}$$

Obviously, depending on the value of $|\rho|$, the enhancement available from the ground plane may range from zero to 12 dB. Ignoring all other factors for the moment, we may estimate how the surface roughness influences the ground plane performance. Returning to Equation (32), we can assume that $|\Gamma| \simeq 1$ and insert the value for $|\rho|$ in Equation (39). We assume that the grazing angle ψ is fixed at the value appropriate to a ray striking the ground plane at the specular point, and this is $\psi = 0.531$ degree.

The calculated results are displayed in Figure 7, which suggests that the surface can be surprisingly rough without degrading the ground plane performance. For example, an RMS surface roughness of 6 wavelengths (0.75 inch at 95 GHz) reduces the ground plane effect by only 2 dB (down to 10 dB from a perfect 12 dB).

Finally, there is a question if the antenna beam is too narrow to fully illuminate both the target and the specular point. As measured from the horizontal, the elevation angle of the direct path from the antenna to the target is

$$\varepsilon_1 = \arctan(h_t - h_r)/G \tag{40}$$

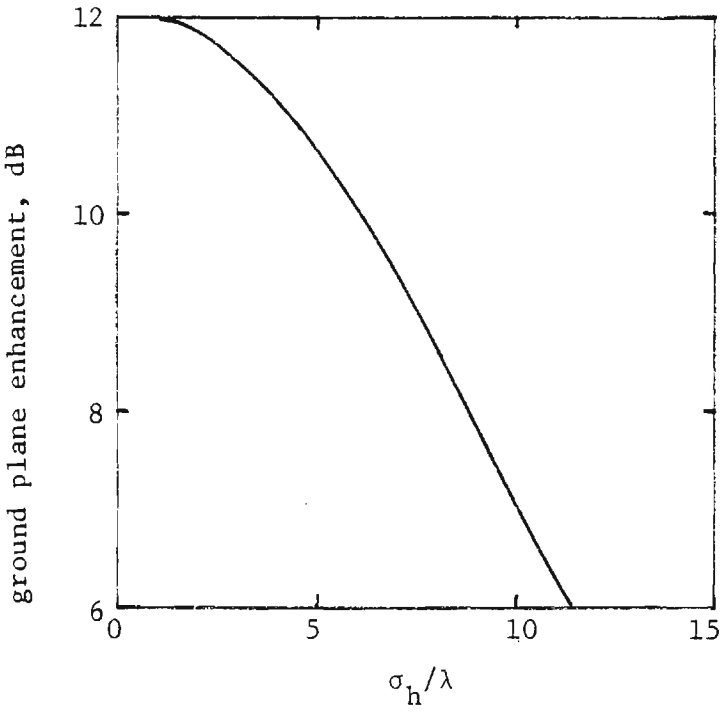

Figure 7. Ground plane performance as a function of the normalized RMS surface roughness.

while the angle from the antenna to the specular point is

$$\varepsilon_2 = -\arctan(h_t + h_r)/G \tag{41}$$

in which the minus sign identifies a depression angle. Thus, the net target illumination arrives from two different portions of the antenna radiation pattern on opposite sides of the boresight axis.

The two amplitudes can be equalized if the boresight is aligned midway between these two directions,

$$\varepsilon_{bs} = \frac{1}{2}(\varepsilon_1 + \varepsilon_2) \simeq -h_r/G \tag{42}$$

However, this angle is too small (-0.01 degree) to be significant and the antenna may be boresighted along the horizontal.

Assuming an 8-inch antenna diameter, we can estimate the relative field strength due to the angular locations of the target and the specular point off the boresight axis. To do so, we will use the mean off-boresight angle,

$$\bar{\varepsilon} = \frac{1}{2}(G_1 + G_2) = 0.521 \text{ degree} \tag{43}$$

We obtain f(w) = 0.715, hence the power radiated at this angle is 2.9 dB below the on-axis radiated power. Thus, for this size antenna, the target and the ground plane specular point both lie very nearly at the half-power points defining the antenna beamwidth.

Ignoring for the moment how a larger antenna could possibly be placed with its center only 3.42 inches above the ground plane, we can perform the same calculation for, say, a 10-inch diameter antenna. We find that the radiated power is down 4.7 dB from the boresight value; this is even worse than for the 8-inch antenna because of the narrowed beam. Thus the use of the ground plane at these very high frequencies restricts the available antenna gain because the beam must be broad enough to adequately illuminate both the target and the specular point.

The boresight gain of an 8-inch diameter antenna is about 43 dB. Since the target and the specular point will be illuminated at levels nearly 3 dB below this value, the net effective antenna gain will be about 40 dB. Assuming a ground plane effectiveness of about 10 dB, the net sensitivity with the ground plane using an 8-inch antenna is about 50 dB. In contrast, we may use a 10 x 30 inch antenna as described earlier without the

ground plane, and the gain of this antenna is about 50 dB. Since the ground plane would not be used, there is no ground plane enhancement.

Thus, equal sensitivities can be obtained with or without the ground plane. The ground plane restricts the size of the antenna that can be used, but the ground plane enhancement compensates for the reduced gain. But the deliberate spoiling of the ground plane effect allows the use of an antenna with higher gain. The decision whether or not to utilize the ground plane therefore depends on other factors.

The dominant feature in a decision to utilize the ground plane effect is the cost of range preparation.

2.4 TARGET SUPPORT STRUCTURE

The absorber covered metal pylons used at Grey Butte to support and rotate test targets are low RCS structures. The canted vane presents a sharp edge to the radar, but the incident rays strike the vane at oblique angles. In theory, there is no return from the main body of the structure and the dominant source of background echo comes from the discontinuity (the rotary head) at the top.

Typically this rotary head is embedded in the target (which must be specially built with an internal mating fixture) and any residual returns can be attributed to the cavity and edges of the aperture cut in the target. The radar echo from a curved edge varies inversely with the radar frequency, hence, if the frequency is increased by a factor of 10, the edge return will drop by 10 dB.

Another source of background return is due to interactions between the target and the support pylon. These are very difficult to measure or to predict because the returns disappear when the test model is removed from the pylon. They depend on the specific geometry of the test target, and even for an explicit configuration, a theoretical analysis would be difficult. Consequently no attempt is made here to estimate the pylon return.

Our guess is that the radar return from the target support structure will be no larger at 95 GHz than it is at lower frequencies, and in all probability, it will be lower.

2.5 ATMOSPHERIC EFFECTS

Although the length of the test range is fairly short (1180 m), the atmospheric effects on the system can be appreciable. From Reference 5 it can be seen that at 95 GHz the attenuation due to the clear atmosphere would be 0.23 dB/km for 100% relative humidity and sea level pressure (worst case conditions). Thus, the round trip attenuation could be no greater than:

$$A_A = 0.23 \text{ dB/km} \times 1180 \text{ m} \times 2 = 0.54 \text{ dB} \quad (44)$$

Thus, the worst effect would be a small calibration error due to changes in relative humidity. However, for rain the effect would be much more severe. From Reference 5 the attenuation due to rain at 95 GHz can be expressed as:

$$\alpha_R = 1.6R^{0.64} \quad (45)$$

where R is the rain rate. Thus, for a 5 mm/hr rain the total path attenuation would be:

$$A_R = 4.48 \text{ dB/km} \times 1180 \text{ m} \times 2 = 10.5 \text{ dB} \quad (46)$$

This is a very significant amount and could strongly affect the system sensitivity. This is confirmed by actual data taken by the Dutch [6] which are shown in Figure 8.

Another effect of the rain would be to backscatter energy to the measurement system. From Reference 5 the backscatter at 95 GHz is 7.5×10^{-5} dB/m. The volume of the beam at the target area can be calculated from

$$V = \frac{\pi}{4}\left(\frac{3 \times 10^8 \times 200 \times 10^{-9}}{2}\right)(0.875 \times 0.0349)(0.875 \times 0.00875)(1180)^2$$

$$V = 7651 \text{ m}^3 \quad (47)$$

Thus the radar cross section σ is given by

$$\sigma = 7 \times V = -2 \text{ dBsm} \quad (48)$$

Thus, the rain backscatter would completely "swamp" the target return. Furthermore, if the target were wet, the RCS of the target would be significantly altered. Fortunately, rain is rare at the Grey Butte test range.

The effects of dust will be primarily backscatter effects since the attenuation will be negligible. From Reference 7, the backscatter coefficient η could be as high as 10^{-8} for extremely heavy dust. Thus, a backscatter radar cross section could be as high as -21 dBsm and could affect the measurements.

Thus, measurements should be suspended during either rain or heavy dust conditions.

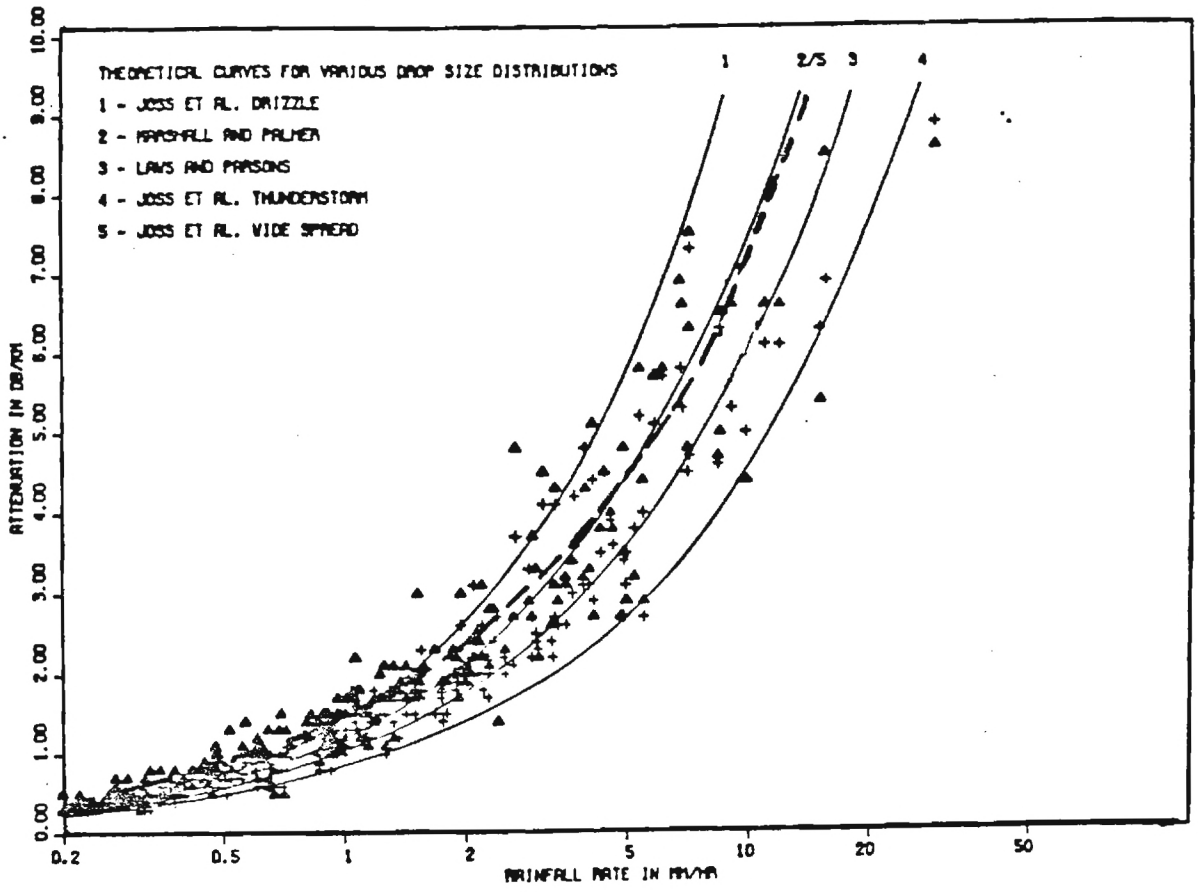

Δ Measured Attenuation
+ Calculated Attenuation Derived from Measured Raindrop Size Distributions
- Rain Attenuation Model

Figure 8. Comparison of rain attenuation model with data and theoretical curves at 94.6 GHz.

SECTION 3
95 GHz MEASUREMENTS RADAR SYSTEM

3.1 GENERAL DESCRIPTION

As discussed in Section 1, selection of the radar system design was based on a preliminary evaluation of three approaches. In the evaluation, both expected performance and development costs were assessed as functions of required and desired system specifications. Based on system specifications and the operational parameters determined by the test range geometry, the extended interaction amplifier (EIA) transmitter with coherent reception and integration was selected as the desired system. A block diagram of the proposed design is shown in Figure 9.

The design selected is fully responsive to the McDonnell sytem requirements and meets or exceeds the desired system performance specifications. A summary of expected system performance is given in Table 8 along with the preliminary specifications. A more detailed discussion of overall performance is provided in the following sections of this report.

3.1.1 ANTENNA SYSTEM

As shown in Figure 9, the proposed system is a bistatic configuration with separate transmit and receive antennas. Based on test range requirements, a fan beam lens antenna was selected and, as discussed in Section 2, the maximum size antenna allowable is approximately 4.5" x 18" with a corresponding gain of 44.5 dB. The two antennas are identical and are connected to the output of the transmitter and the input of the calibrator by a dual polarization subassembly. This subassembly consists of a remotely controllable solenoid waveguide switch (with proper termination), an orthogonal-mode transducer (dual mode coupler), and a circular-to-rectangular waveguide transition. The transducer allows propagation of two linearly, orthogonally polarized signals through the same antenna and feed assembly with high isolation ($\geq$ 30 dB) between paths while the transition converts the TE_{11} mode in circular guide to the TE_{10} mode in rectangular guide and vice versa. By switching between the vertical and horizontal ports of the transducer, measurements of all components of linear polarization (i.e., HH, HV, VV, VH) can be made. The polarization subassembly is made up of off-the-shelf items from TRG, while the lens antennas will be designed and fabricated by Georgia Tech. A number of

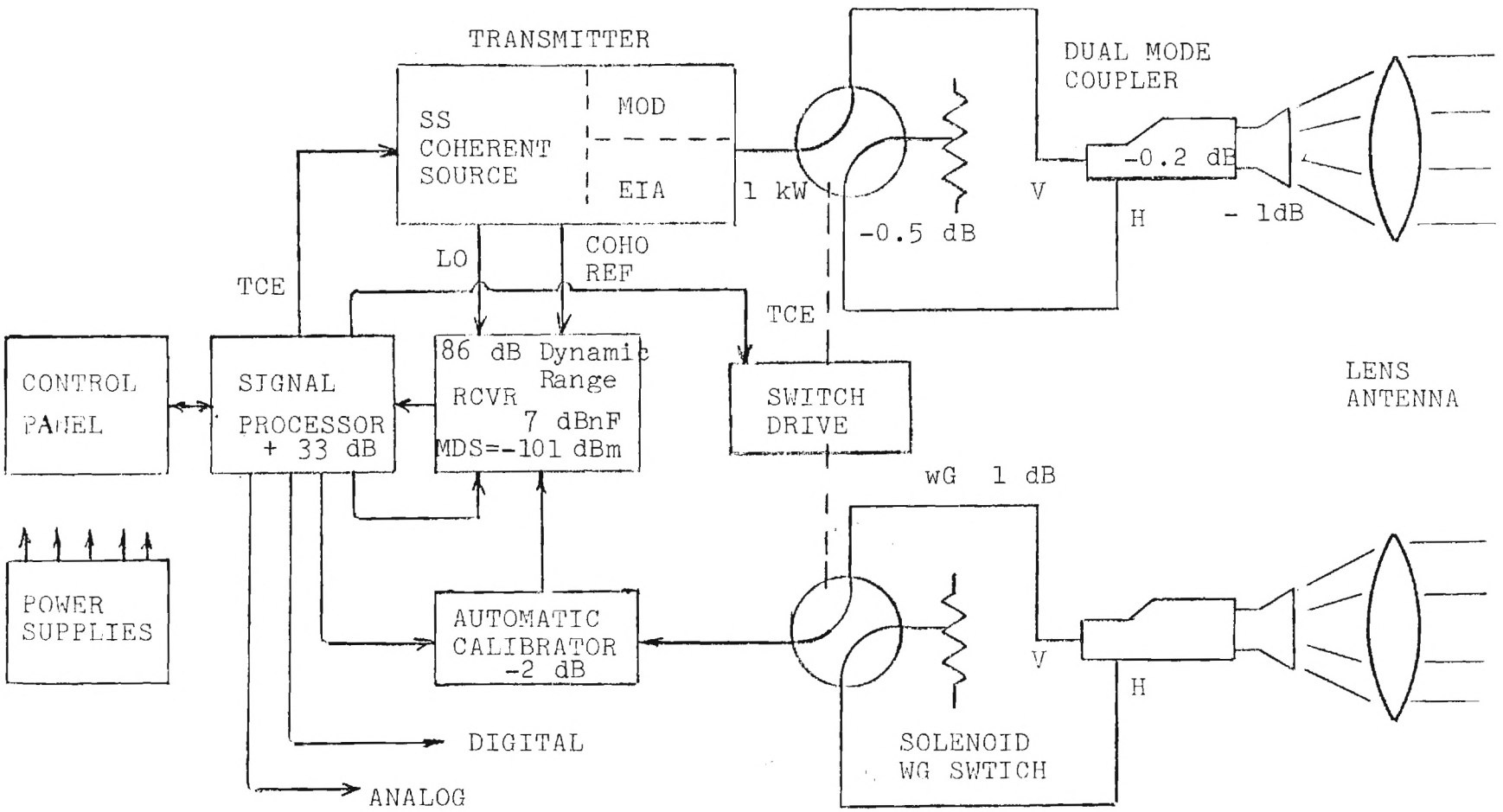

Figure 9. Annotated block diagram of measurement radar showing system sensitivities/losses.

similar systems have been built by Georgia Tech for both sponsor and internal use. The various components are listed Table 9.

TABLE 8. 95 GHz RADAR PARAMETERS

Parameter	Specification	Proposed Design
System Sensitivity	-50 dBsm Required -60 dBsm Desired	-67 dBsm
Dynamic Range	60 dB Required 80 dB Desired	86 dB (Receiver) 72 dB (Processor)
Polarization (Remotely Switchable)	HH VV	HH,HV VV, VH
Calibration	Automatic	Automatic 0 to 100 dB
Outputs	Analog Digital	Analog Digital
Peak Power	--	1 to 2 kW Coherent
Pulse Width	200 ns Minimum	400 ns
PRF	Synchronous to 1 kHz	21 kHz
Antenna Gain	--	44.5 dB
Beamwidth	--	2.0° Az 0.5° El
Receiver Type	--	Superheterodyne Linear 4 MHz Bandwidth Centered at 500 MHz
Dynamic Range		86 dB Instantaneous
Detection		Synchronous I & Q Coherent
NF		7 dB
Sensitivity		-101 dBm

TABLE 9. ANTENNA/FEED ASSEMBLY COMPONENTS

Component	Quantity	Manufacturer	Model
Lens Assembly	2	Georgia Tech	N/A
Dual Mode Coupler	2	TRG	W881
Transition	2	TRG	W884
Waveguide Switch	2	TRG	W535

The antenna system will be nonscanning with provisions for boresight alignment adjustments to be made in the field. No provisions for steering the system have been included in the proposed design, and it is assumed that McDonnell will provide a steerable platform if one is required. Also, the design is based on the assumption that polarization switching will be limited to switching between measurement runs (or will be switched at a fairly low speed). Switching times are limited to a minimum of 0.5 second by the solenoid waveguide switch.

3.1.2 TRANSMITTER DESCRIPTION

The transmitter design as shown in the overall block diagram combines the low power coherent solid state (SS) approach with a high power Extended Interaction Amplifier (EIA) output stage. This approach provides 1-2 kW of coherent power at 95 GHz to the input to the solenoid waveguide switch, which in turn selects the RF port for transmission of either vertical (V) or horizontal (H) polarization. The SS source/driver design is based on a demonstrated Hughes Aircraft Corporation (HAC) approach using Impatt injection locked oscillators (ILO) to achieve a coherent reference for the receiver and coherent drive power for the EIA. The EIA design is based on recent work at Georgia Tech in developing EIA modulators and on the recent effort of Varian of Canada in developing grid modulated EIA's. Thus, the transmitter design combines state-of-the-art but proven technology involving SS, EIA, and modulator developments to achieve a high power coherent transmitter at 95 GHz. It is anticipated that the SS coherent source as

well as the receiver would be developed under a subcontract to Hughes Aircraft Company, the EIA would be purchased from Varian, and the modulator would be developed by Georgia Tech. Each of these developments is described below.

3.2 SOLID STATE TRANSMITTER DRIVER/COHERENT RECEIVER

3.2.1 SS COHERENT SOURCE/DRIVER

A block diagram of the SS coherent source/driver is shown in Figure 10. The RF front end uses a low noise crystal oscillator at approximately 100 MHz as the stable master oscillator (STAMO) for the system. One of the most important characteristics is the low phase noise which is shown plotted in Figure 11. The STAMO output is fed to a two-stage power divider; one arm provides the coherent reference to the 95 GHz phase-locked Gunn oscillator, the other arm provides coherent drive to the IF oscillator. The IF oscillator is a X5 multiplier which generates a signal at 500 MHz to provide the IF input to the single-sideband (SSB) generator and the local oscillator (LO) signal to the synchronous detectors in the receiver.

The phase-locked Gunn oscillator uses a bias-tuned Gunn oscillator in conjunction with a phase-lock multiplier and locking electronics to achieve a coherent output at 95 GHz. This signal is split by a two-way power divider to provide the LO signal to the millimeter wave mixer in the receiver front end and the LO input signal to the SSB generator. The LO signal for the SSB generator is amplified (without phase noise degradation) by a CW Impatt injection-locked oscillator (CW ILO) before it is applied to the SSB generator LO port.

The ILO is designed to be free-running at the same frequency as the Gunn oscillator and is injection-locked to the Gunn. The locking gain is typically 15 dB over a $\pm$ 200 MHz bandwidth. A typical plot of locking gain versus bandwidth is shown in Figure 12. The output from the ILO is approximately +20 dBm, and past measurements have shown that low phase noise is maintained throughout.

The SSB generator is basically a double-balanced mixer with an output filter designed to reject the LO frequency and the lower sideband frequency. Thus, the output frequency (95.5 GHz) is the sum of the 95 GHz LO and the IF at 500 MHz. The IF input is pulsed (attenuated by 60 dB) by a PIN switch that is synchronized to the transmitter PRF so that the SSB generator provides a pulsed output of approximately 400 ns at a 21 kHz PRF. This output provides the input to the EIA driver amplifier which is a pulsed Impatt injection-locked oscillator (PILO). The PILO stage is modulated at the system

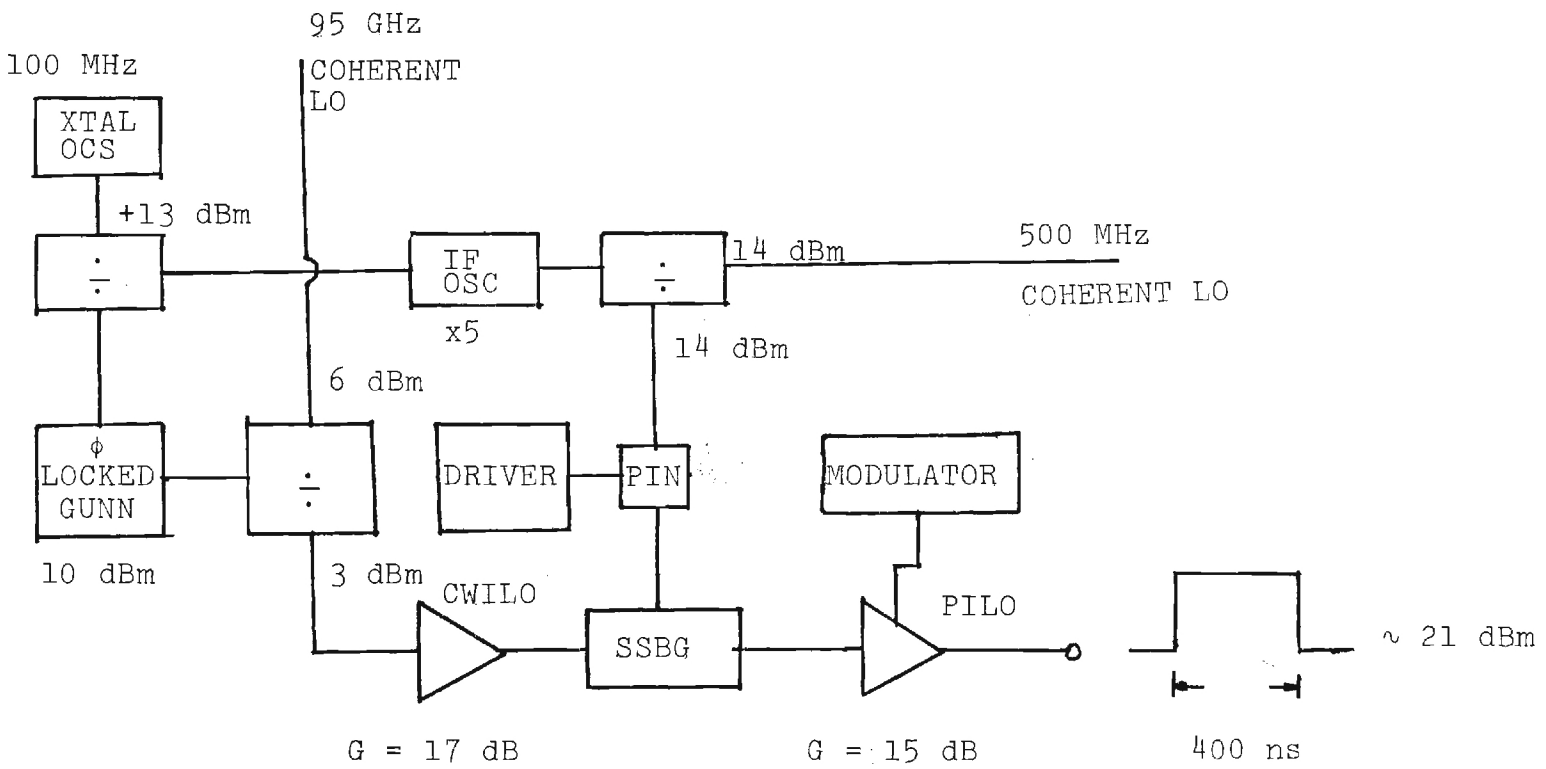

Figure 10. Solid state coherent source/driver.

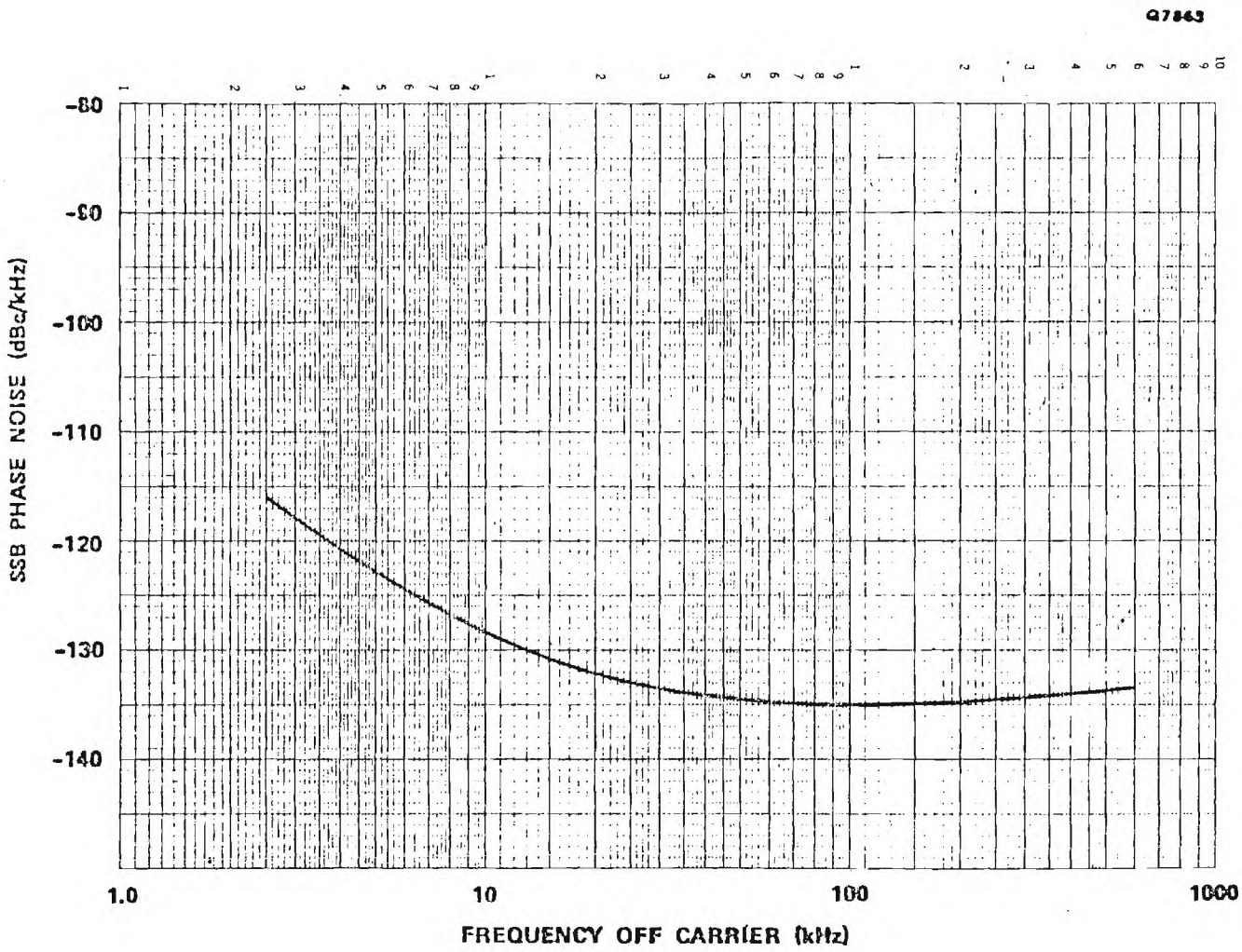

Figure 11. SSB phase noise of 104.666 MHz crystal oscillator. (From reference 8)

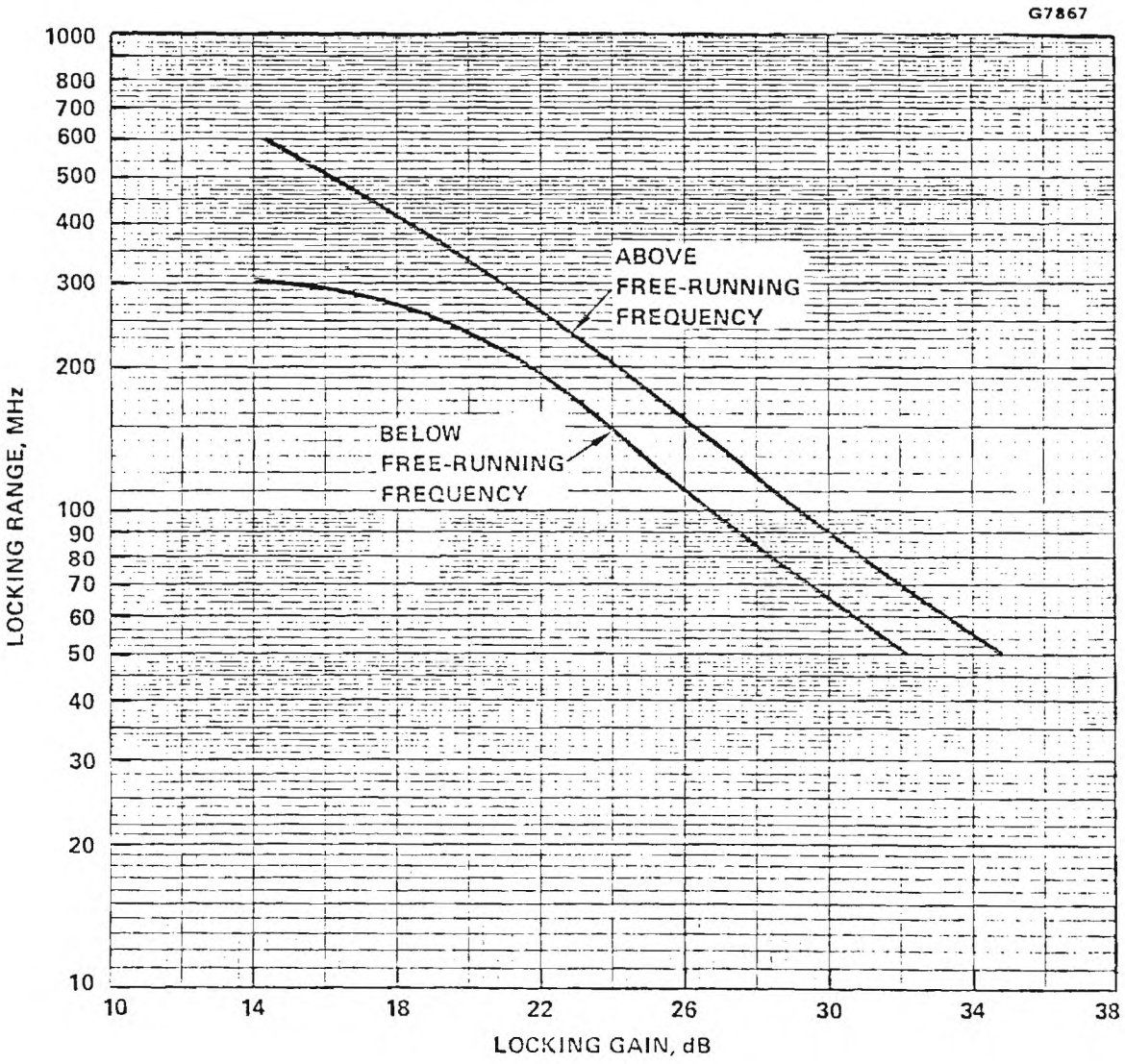

Figure 12. Locking gain-bandwidth characteristics of transmitter CW IMPATT ILO. (8)

PRF rate which, along with pulsing of the SSB generator, minimizes the possibility of feeding in-band and out-of-band signals to the tube amplifer (or the receiver) during interpulse periods.

The coherency of the pulsed ILO has been measured and is shown in Figure 13. This figure shows the oscilloscope display of the output of a phase detector used in a phase bridge measurement of additive phase noise. The triple exposure corresponds to a phase shifter reading of -90 degrees (top), 0 degrees (middle), and +90 degrees (bottom). Coherency is demonstrated by the fact that there is a single trace corresponding to many pulses. This particular PILO has 5 watts of output power and is operated at a PRF of 60 kHz and a pulse width of 100 microseconds.[9] The PILO is the final output of the SS driver and will provide a coherent drive signal to the high power EIA output stage. The PILO is specified at +23 dBm output for a 400 microsecond pulse width and a 21 kHz PRF.

3.2.2 COHERENT RECEIVER DESCRIPTION

The receiver block diagram is shown in Figure 14 along with the SS portion of the transmitter. The receiver consists of two precision attenuators in series (calibrator), a mixer/preamplifier, an IF narrow-band filter, and four parallel IF/video channels. The four parallel channels are required to achieve the in-phase (I) and quadrature (Q) processing of the coherent signal for two gain settings. Since synchronous detectors are used in the I and Q processing, amplitude and absolute phase (coherent reception) information is retained. Ideal integration gain is realizable by later integrating and recombining the two (I and Q) signals.

The inputs to the receiver are the RF signal from the antenna/polarization assembly and coherent RF and IF LO drive signals to the mixer and synchronous detectors. The output signals to the processor are low level and high level I and Q information from the four parallel video amplifiers. The design provides an instantaneous dynamic range of 86 dB and a receiver sensitivity of -101 dBm. The general operation and design of the receiver are discussed in the following paragraphs.

Starting at the RF input, the received signal passes through the two precision attenuators before being applied to the mixer. These attenuators provide a means by which the system amplitude response can be determined and calibrated. At various times, depending on the amount of drift in the system and the data accuracy required, the system is operated with a known reference target representing a radar cross section

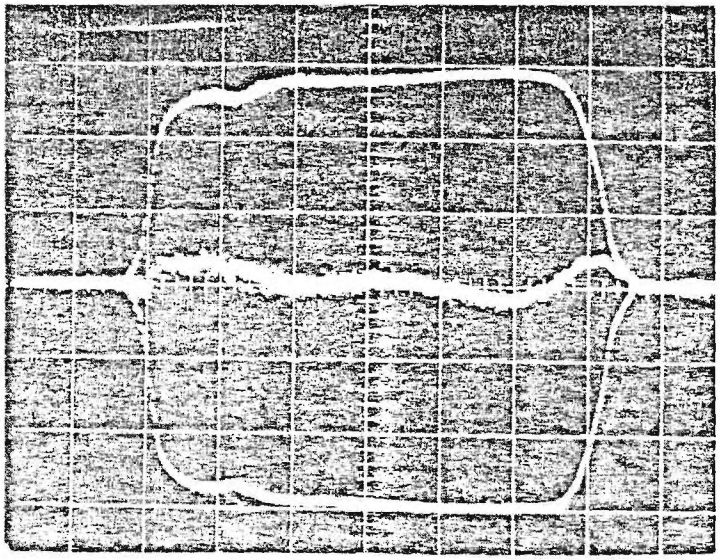

HORIZONTAL: 10 NSEC/DIV.

Figure 13. Phase detector output with ILO locked at center frequency (94.6 GHz). (From reference 2)

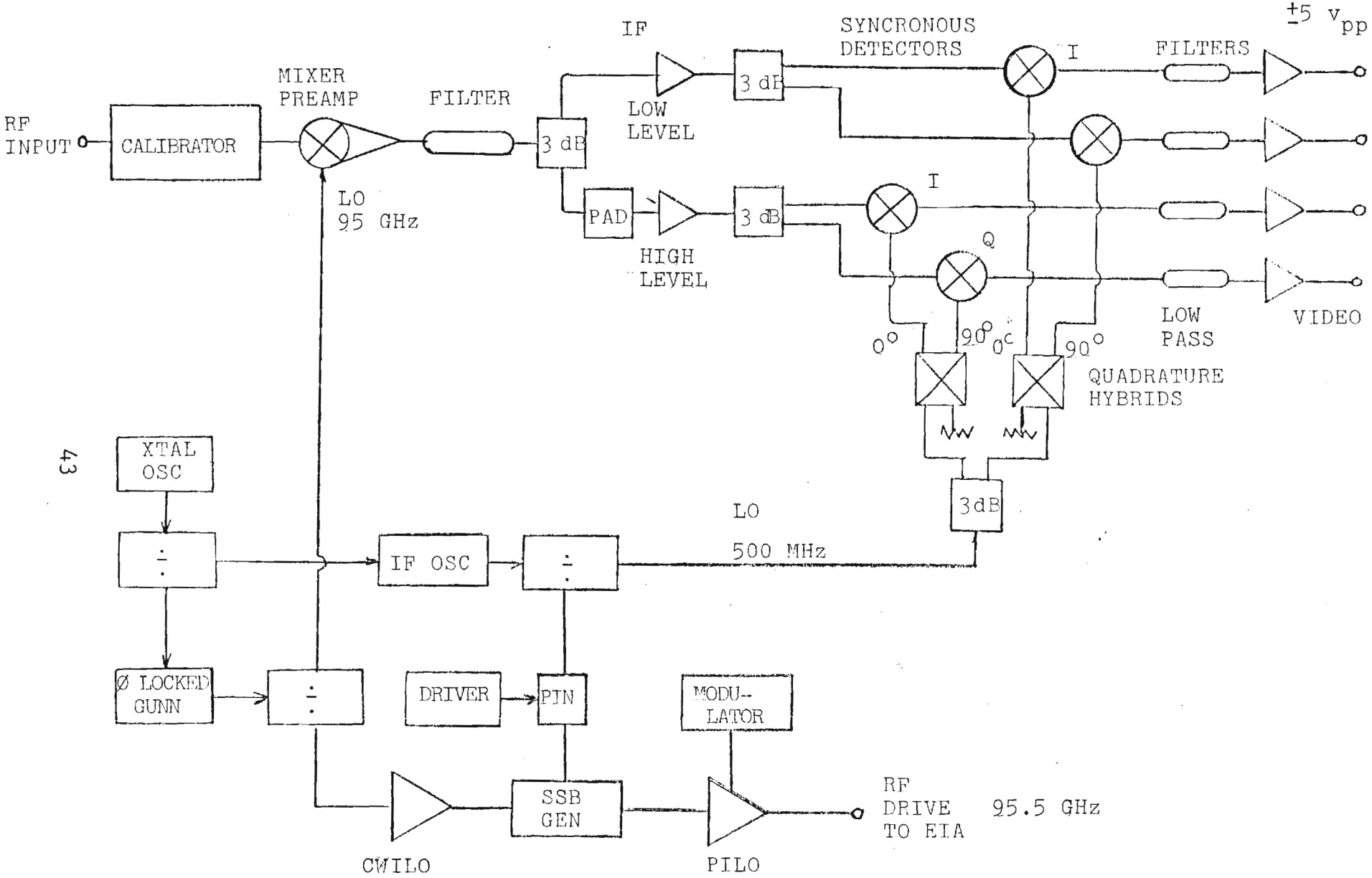

Figure 14. SS Driver - Receiver block diagram

as large as the largest target radar cross section expected. While the system is operating, the precision attenuators are used to insert known amounts of attenuation in 5 dB increments from 0 to 80 dB. The system response is recorded over this range and represents the calibration curve for the system. This information is "read" by the radar calibration and linearization circuits, and the system is self-calibrating as long as the information remains in memory. The details of the automatic drive design and the processing of the data for the calibrator are covered in Section 3.3.7.

In the normal measurement mode, the attenuators are set to 0 dB, and the received signal which is centered at 95.5 GHz is applied to the RF port of the mixer. The LO signal is derived from the phase-locked Gunn oscilator (transmitter section) and is fixed at 95 GHz. The resulting intermediate frequency (IF) is about 500 MHz. The noise bandwidth of the IF/video section is set by appropriate use of two filters. A 4 MHz bandwidth Chebychev filter centered at 500 MHz follows the mixer/preamplifier; this filter bandwidth was selected for low phase distortion of the 400 microsecond RF pulse (as opposed to a 2.5 to 3 MHz filter). In addition, video filters adjusted for optimum noise bandwidth and low distortion are used at the output of each synchronous detector. The selection of these filters will ensure low phase distortion at minimum noise bandwidth and, with the mixer noise figure of 7 dB (SSB NF), determine the receiver sensitivity.

Since coherent integration of a large number of pulses is required, linear processing is necessary and, therefore, a linear receiver is perferred. Typically, linear IF amplifiers have a limited instantaneous dynamic range of 50 to 60 dB and require an AGC to achieve the 60 to 80 dB dynamic range specified. Due to the possibility of large changes in target signal return from a rotating target at these high frequencies (i.e., during integration time), an instantaneous 80 dB dynamic range is much perferred. The required 80 dB dynamic range is achieved as follows. The input signal from the IF filter is equally divided via a 3 dB coupler and two parallel channels are used. The upper channel (low level channel) has the signal fed directly to the IF amplifier, and the bottom channel (high level channel) uses an attenuated signal input to the IF amplifier. The individual channels process the lower and upper 40 dB signal range, and selection of the proper video output is determined by monitoring the signal from the low level IF amplifier.

Following the IF amplifiers, the signals are again split via 3 dB couplers to provide the inputs to the I and Q synchronous detector channels. Maximum information is retained by providing synchronous detection for both the I and Q channels. Quadrature

detection is facilitated by using quadrature hybrids which provide 3 dB coupled, 0^{o} and 90^{o} phase shift signals to the detectors from the 500 MHz coherent reference. After detection, the signals pass through low pass filters and are amplified and buffered by the video output amplifiers, then input to the sample and hold circuitry in the processor.

The overall system gain established for the receiver is based on the maximum input signal at the RF front end (1 dB compression points for the preamplifier), the nominal output from the video amplifiers ($\pm$ 5.0 V_{pp}) and the maximum input power level of the synchronous detector. The maximum input level to the synchronous detector is restricted to -5 dBm or less to ensure optimum system linearity. With this criterion, the gain of the video and IF amplifiers and the value of attenuation pad preceding the IF amplifier may be determined.

The mixer/preamplifier selected has a typical 1 dB compression at +5 dBm output for a 20 dB gain. Therefore, the maximum signal level which can be accurately measured is -15 dBm at the RF input (the MDS is approximately -101 dBm). Refering to Figure 15, for the high level channel, a maximum of - 5 dBm input to the detector determines the overall pad-amplifier gain to be -2 dB. If the desired range of the high level channel is 40 dB, then the maximum signal level to be processed by the low level channel is -35 dBm from the mixer/preamplifier. This implies an IF gain of less then 38 dB. Since it is not necessary to split the dynamic range between the two channels by 3 dB, a cost trade off can be made in the final selection of the IF amplifiers and pad required without degradation of system performance.

Returning again to the maximum allowed input to the synchronous detectors, the video gain can be determined. For a $\pm$5 V_{pp} output and assuming a total of 7 dB loss through the detector and filter, the video gain (maximum) is set at 36 dB for a maximum detector input of - 5 dBm.

3.3 SIGNAL PROCESSOR/CALIBRATOR

Both the Inphase and Quadrature coherent receiver channels must be processed by the system to realize the full advantage of coherent integration in signal-to-noise ratio improvement. If 2048 pulses are integrated, a coherent integration improvement of 33 dB will be realized. An average improvement of 30 dB will be realized if only one of the two channels is processed. Note that a gain of only 16.5 dB will be realized if post detection (non-coherent) integration is used. Once a decision is made to take advantage of the coherent gain available, only a marginal increase in cost is incurred for processing both I and Q channels to obtain the additional 3 dB gain.

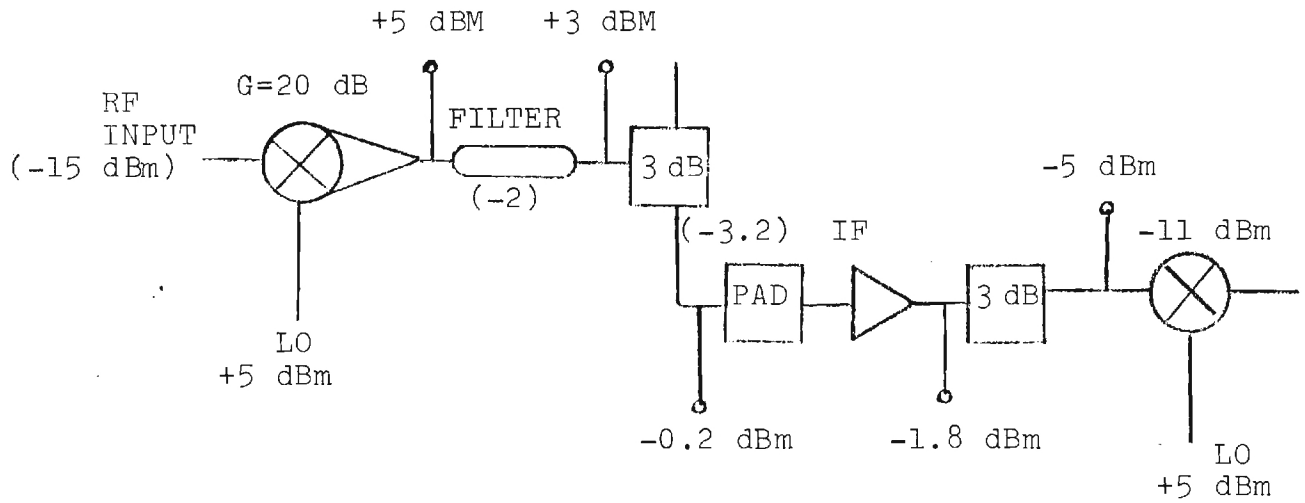

Figure 15. Maximum receiver high level signal levels.

The four signals out of the receiver represent the I and Q components for the high level and low level channels. At present, it is thought that the difference in signal level should be 40 dB, but further study during a detailed design phase of development may lead to a change in this value to achieve optimum performance.

The sequence of signal processing operations is as follows:

1. Sample-and-Hold Process
2. Analog-to-Digital Conversion
3. Integration
4. Recombine I and Q Channels
5. Apply Calibration Factor
6. Conditioning Output Signal

Figure 16 shows the block diagram of the signal processor. The various processes can be described as follows:

3.3.1 SAMPLE-AND-HOLD PROCESS

There are no particularly stringent requirements for the sample-and-hold function. There are a variety of commerically available circuits which will perform the task adequately. The use of a 4 MHz bandwidth to match the 400 ns pulse width ensures that there will be adequate bandwidth to pass the entire pulse energy. A sampler having a 200 ns acquisition time will be adequate. It is important to operate analog functions at as high a signal level as possible to minimize the effects of noise. A signal level of ± 5 volts is proposed for the sampler input. If a 12 bit A/D converter is used after the sampler, and the A/D conversion process takes 4 μs, then the least significant bit (V_{LSB}) represents

$$V_{LSB} = \frac{V_{fs}}{2^N} = \frac{10}{4096} \simeq 2.5 \text{ mv} \tag{48}$$

where V_{fs} is full scale voltage
N is number bits.

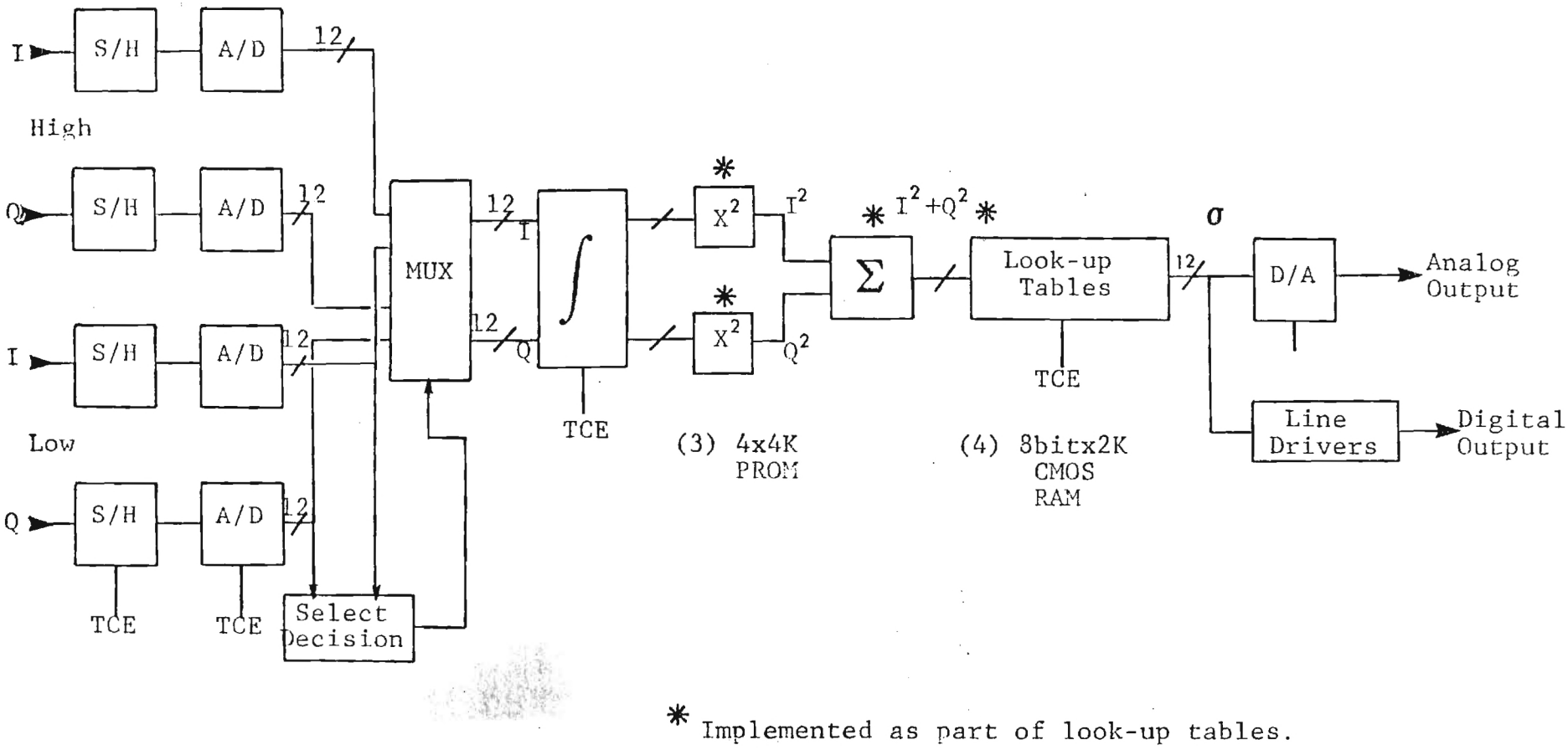

* Implemented as part of look-up tables.

Figure 16. Block diagram of radar signal processor.

In this case, we cannot allow the droop in the sampler to approach 2.5 mv in 4 μs. If we arbitrarily set the maximum droop to 0.2 V_{LSB}, then the droop rate is limited to 0.5 mv/4 μs = 125 μv/μs. Available sample-and-hold circuits having maximum droop rates of 50 μv/μs are fully adequate for our application.

3.3.2 ANALOG-TO-DIGITAL CONVERTER

There is no particularly stringent requirement for the A/D converter, except that 12 bit integrity is required and a 4 μs conversion time is desired (to keep the droop during conversion to a minimum). Units having a ±5 volt input and a 4 μs conversion time are commerically available. One of these will be selected for the application.

3.3.3 INTEGRATOR

One integrator can be used to process all parallel channels. An adder (74LS283 or equivalent) is used to accumulate the sums of the specified number of pulses (in this case, 2048), and a register is used to store the sum for each channel. The parallel data are fed into the input of the integrator serially using either a multiplexor or a parallel-to-serial register. The output of each output register enables parallel access to each accumulated number. Figure 17 shows a block diagram of the integrator.

3.3.4 I AND Q CHANNEL RECOMBINATION

In the receiver section, the target signal was separated into the two orthogonal components (I and Q). These two quantities must be recombined vectorially to determine the true cross-section of the target. This requires squaring each value and adding them. Since there is a known relationship between a number and its squared value, a single programmable read-only-memory (PROM) can be used. This is simpler and faster than using a multiplier, although a multiplier would be an acceptable alternate approach. The squarer can be used sequentially in a manner similar to the integrator.

3.3.5 CALIBRATION

It is possible that some non-linearities and drift (due to aging, etc.) exist in the radar transmitter and receiver, such that a true cross section value for the target cannot be precisely determined from the integrator output without calibrating the system. A look-up table is used to compensate for these potential sources of error. This table of values is calibrated during the calibration procedure described in Section 3.3.7. Under

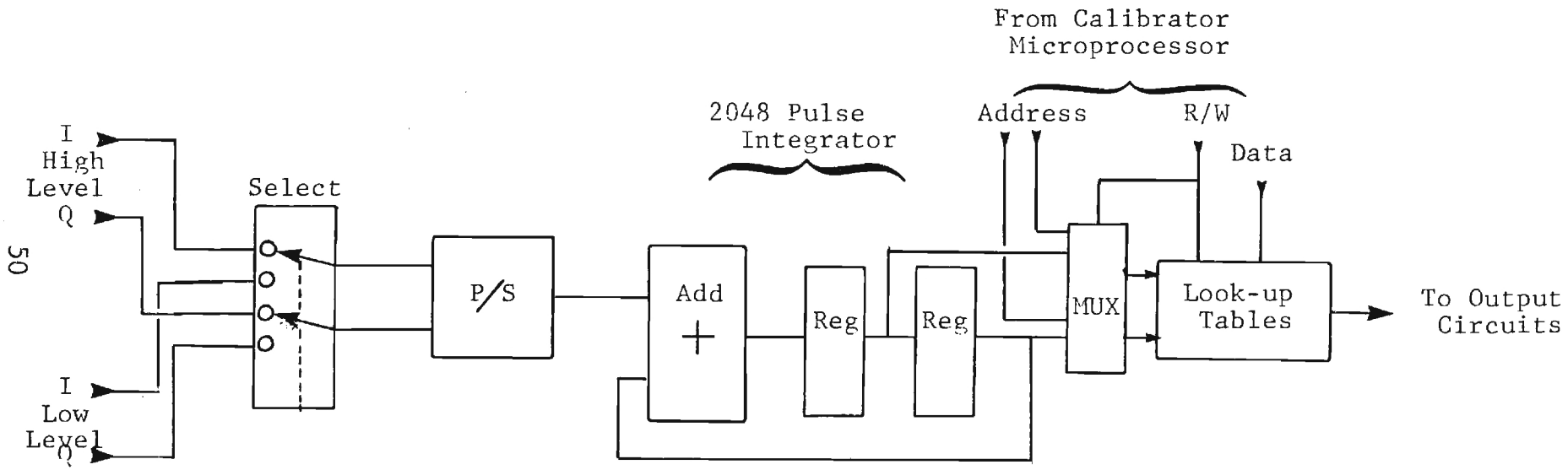

Figure 17. Block diagram of integrator circuit.

ideal conditions, the output number would be the same as the input number, indicating that no non-linearities exist and no change in transmitted level or system loss occurred due to aging or environmental conditions. Such is probably not the case. The look-up tables "learn" the radar characteristics in the calibration mode and "remember" these characteristics in a random-access-memory (RAM). The power supply for the RAM is derived from a nickle-cadmium battery which is continually kept charged, so that the RAM does not lose its memory during the times that the power is off.

3.3.6 OUTPUT CIRCUITRY

The radar can provide a variety of output signals, analog and digital. For example, the analog output could be proportional to target cross-section or proportional to the log of the target cross-section. The digital output could be either a parallel word or a serial data line, or both, depending on the particular needs of the user. Implementation of any of these or similar output modes is relatively straightforward. Details of the exact requirements would be worked out during early stages of system development.

3.3.7 AUTOMATIC CALIBRATION

The output from the radar system is a signal, either analog or digital (or both), representing the radar cross-section (σ) value for the target being evaluated. The value that the radar measures to determine the radar cross-section of a target is the power reflected from the target and captured by the receiving antenna. Many factors in addition to σ contribute to the power received by the receiver. All of these factors must be considered in determining the target radar cross-section. Consideration of these factors involves calibrating the radar system.

Generally, two techniques are employed for calibrating a radar system: a signal generator calibration and a reference reflector calibration. A signel generator calibration involves injecting a sequence of known signal levels into the receiver and measuring the receiver response. The appropriate form of the radar equation is then used to relate the input signal level to target radar cross-section. Several sources of error associated with this technique, particularly pertinent at 95 GHz, make the use of this technique unadvisable except for periodic performance verification purposes. They are, among others:

1. Non availability of stable signal sources at 95 GHz.
2. Inability to match the spectrum of the actual transmitter signal.
3. Inability to account for long term drift in transmitted power, transmitter losses and atmospheric losses.

The preferred calibration technique for this application involves the use of a standard reference target. The radar is boresighted to the reference reflector (a sphere or trihedral of known cross section) which is at the same range as the target to be evaluated. The radar receiver response to a variety of target sizes is measured. In most cases, only one size reference is used (at least as large as the largest expected target value) and smaller sizes are synthesized by inserting prescribed amounts of attenuation into the receiver. This is done by incrementing a precision RF attenuator through its range, at least as far as the expected dynamic range of target values.

Classically, the process has been to record the receiver response to this range of cross section values and also record the receiver response to the target or targets of interest shortly thereafter. The actual target cross-section values are determined during the data analysis phase by comparison of the target data with the calibration data.

In the system described herein, it is suggested that an automatic and built-in calibration system be used. This system basically follows the procedure associated with the reference reflector approach, except that, instead of recording the receiver response to the range of reference values, actual cross-section values are calculated and loaded into a digital memory. The addresses for the memory locations are the values out of the receiver for the various cross section values. The data for the memory are the associated cross-section values themselves. During the calibration cycle, the cross-section values (data) are written into the various address locations and stored. During the data collection cycle, these values are read out and sent to the recorder for plotting or display.

Since the precision attenuators are incremented through their range in relatively coarse (3 dB or 5 dB) steps, not every memory location is loaded with actual cross section data. The points in between the actual measured points are "filled in" by interpolating between measured points.

The system described herein uses remotely controlled attenuators to avoid the need for an operator to manually control the precision attenuators (and avoid the potential for error in setting the attenuators. Two attenuators are required to cover the entire 60 dB

(or 80 dB) range of calibration since each attenuator has a maximum range of 50 dB, and the last 10 dB (40 to 50 dB) is subject to more errors than the lower values. A stepper motor provides the capability to position the attenuators to any prescribed value, and an optical encoder provides a means to accurately determine the attenuation values. An extra degree of sophistication which may be desired would involve calibration of the attenuator/encoder network using references traceable to the National Bureau of Standards.

Automation of the entire calibration procedure is simplified by the use of a microprocessor (one candidate is the Rockwell AIM 65 using the 6502 central processing chip). The functions of the microprocessor are to automatically control the RF attenuators (to position them via the stepper motor and optical encoder feedback to the various attenuation settings), provide the cross section data to be written into the RAM for the calibration points, perform the interpolation routine required to determine the intermediate data points, and provide the RAM with these points. All of this procedure will occur automatically upon operator command. Figure 18 shows a diagram of the radar system with the calibration system, and Figure 19 shows the details of the calibration system itself.

Once the RAM has been "loaded" in the manner described above, it is ready to be used in the data collection mode. The radar receiver and processor output provides the address numbers which are used to recall the appropriate cross-section values as described in the signal processing section. It should be noted that the technique described allows the operator to remotely insert attenuation of any required value, if desired.

3.4 HIGH POWER EIA OUTPUT STAGE

The EIA transmitter stage will provides a stable, reliable pulsed source of millimeter wave power from the Varian Canada, VKB 2449T1, Extended Interaction Amplifier (EIA). RF performance will be optimized at a 400 ns pulse width and 21 kHz pulse repetition rate while providing for safe operation.

3.4.1 MECHANICAL CONFIGURATION

The high power transmitter consists of the EIA integrated with the modulator/high voltage power supply unit as shown in Figure 20 in which the approximate overall dimensions of the units are indicated. the EIA is mounted directly on the modulator to

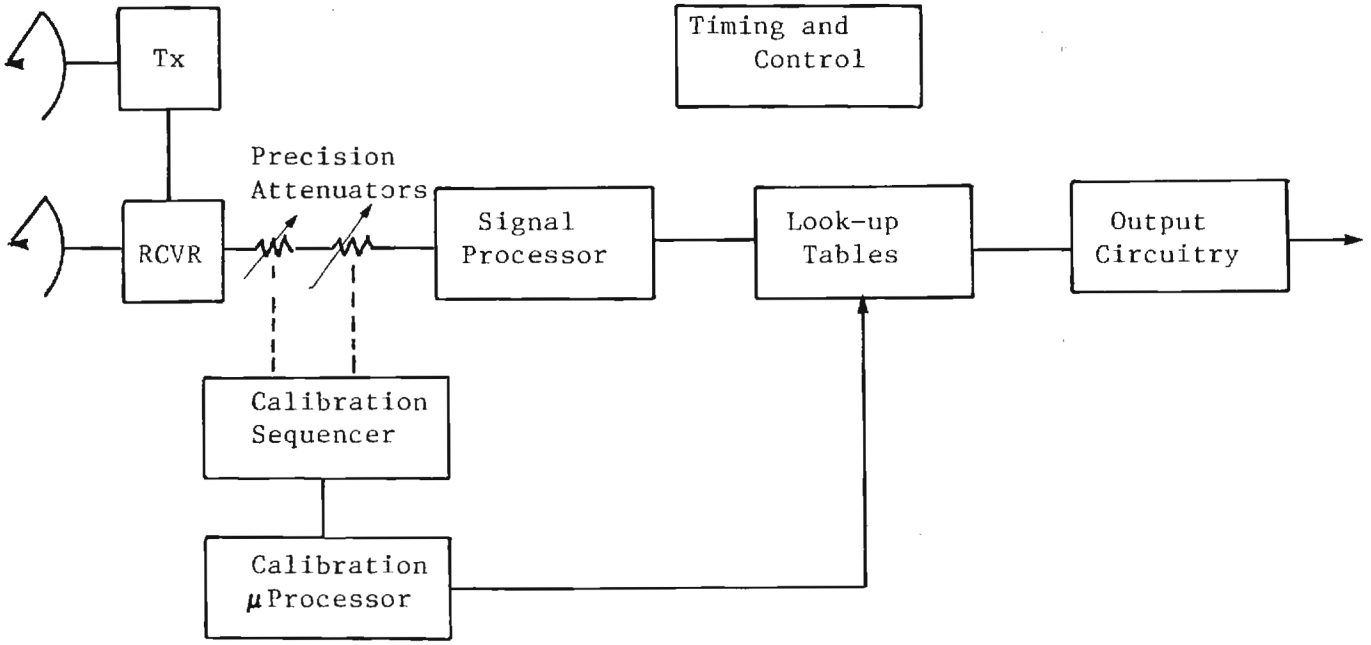

Figure 18. Calibration system as part of the radar.

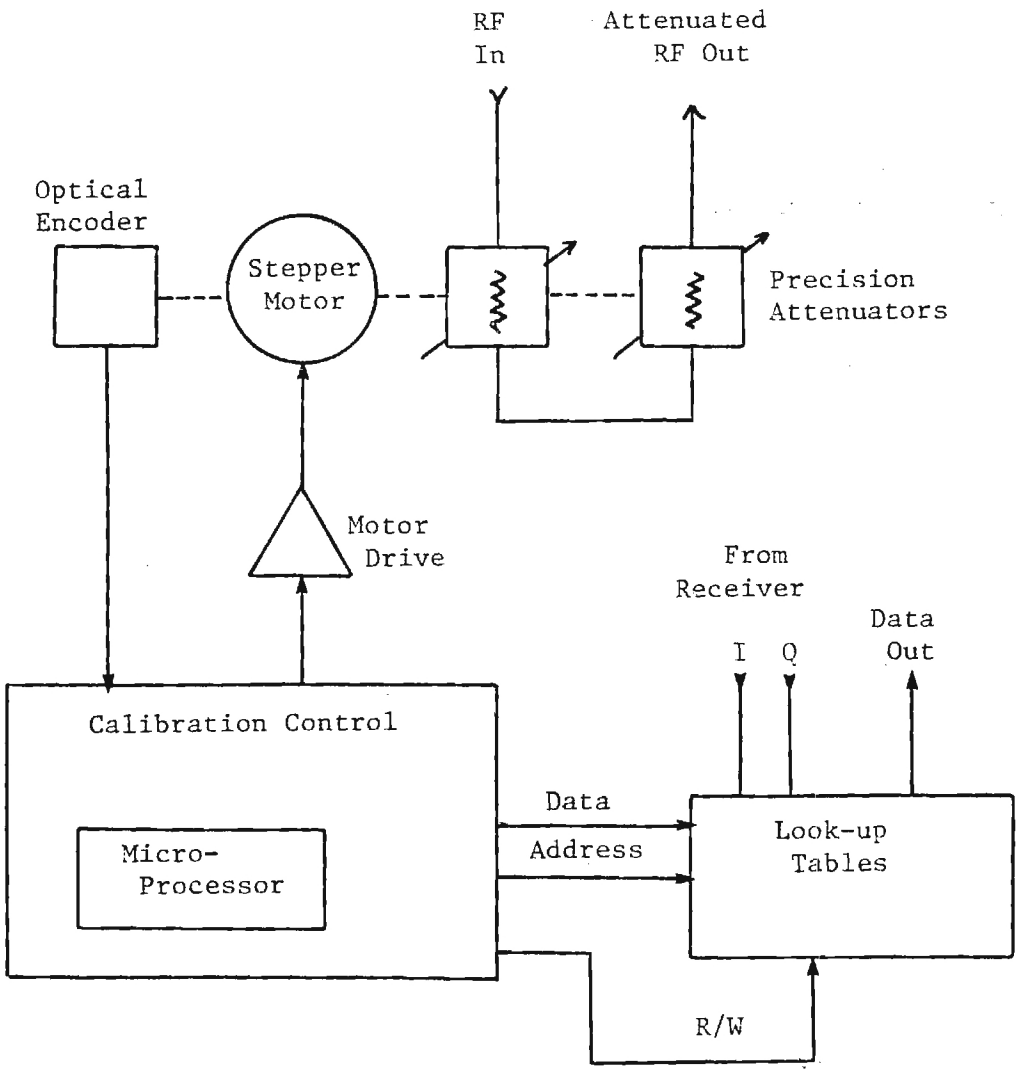

Figure 19. Calibration circuits.

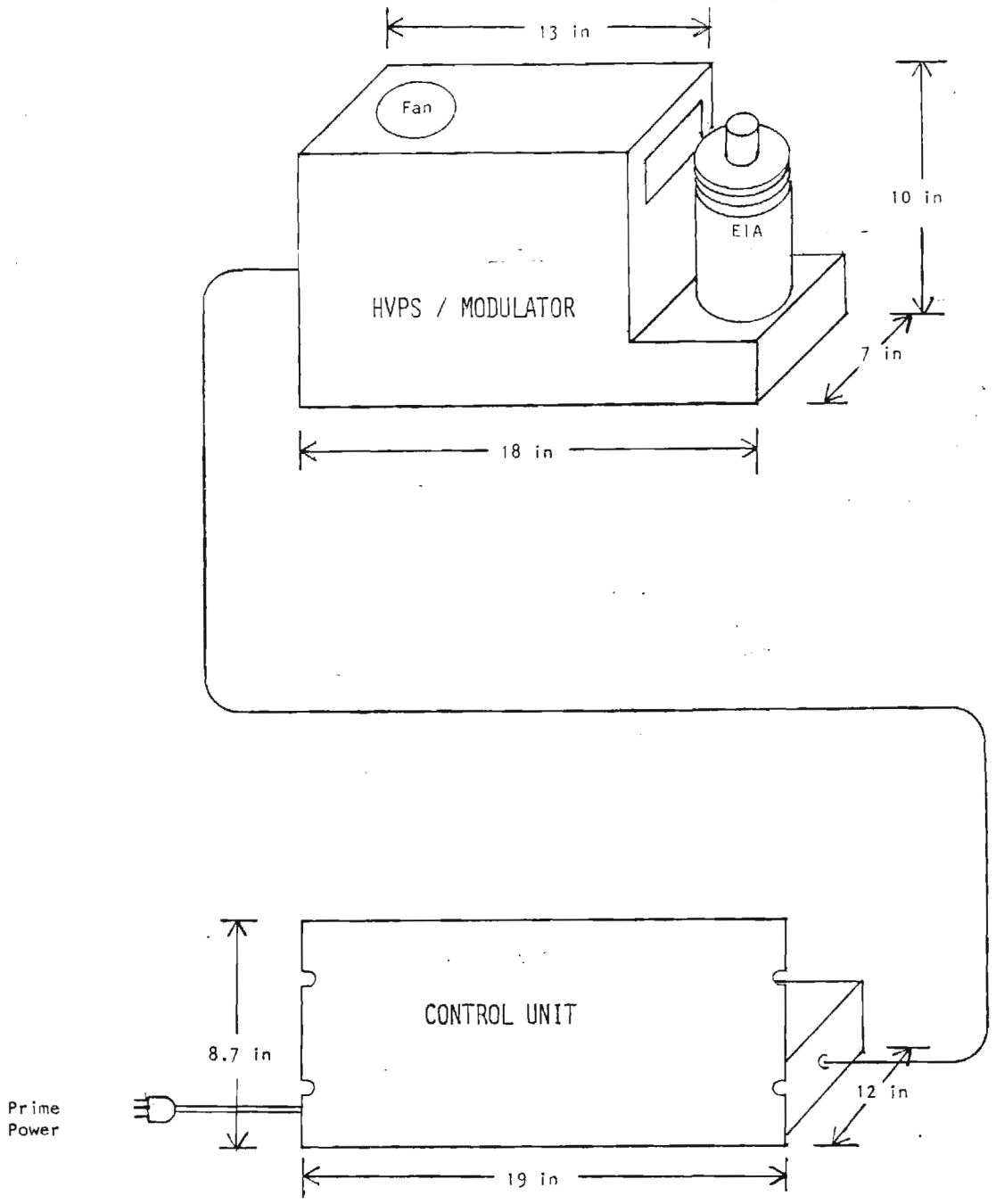

Figure 20. EIA transmitter configuration.

reduce interference from the high voltage pulser. Forced air cooling is also provided from the modulator. The transmitter is operated by applying +28 VDC to the modulator unit along with TTL level control signals. Status and fault signals are also provided to allow easy integration of the transmitter with the radar system. A control unit, which can be rack mounted, is provided for stand alone operation of the transmitter with manual pulse width, PRF, standby, radiate and fault/clear controls. The unit includes +28 V and +5 V power supplies for operation from 110 V/220 VAC 50 to 400 Hz single phase power. The EIA beam voltage and current are displayed on an analog meter.

3.4.2 MODULATOR/POWER SUPPLY DESIGN

A simplified block diagram of the transmitter is shown in Figure 21. The control signals and low-voltage power lines are fed to the modulator through the power cable while the pulse control signal requires a 50 Ω coaxial cable. A power control circuit in the HVPS applies, on command, the required voltages to the EIA and modulator in proper sequence and with the required delay times. The voltages are also removed on command from the operator, or automatically in the case of a tube or modulator fault. The HVPS is a solid state, well-regulated, DC to DC converter with low energy stored to prevent damage to the RF tube in the event of a tube arc. The stored energy in the HVPS and modulator is less than 2.0 joules.

The modulator provides the pulse voltage to the grid of the EIA from the DC power supplied by the HVPS. The modulator consists of a floating hard tube pulser which brings the grid of the EIA from the -24 kV cutoff voltage to the -21 kV cathode operating potential. The hard tube pulser shown in Figure 22 is a push-pull design which gives fast rise and fall times with low power dissipation. The tubes are ruggedized ceramic-metal planar triodes. The pulser is controlled by the solid state pulse driver circuit which converts the TTL level pulse control signal into a 200 volt shaped pulse which is coupled through a high-voltage isolation transformer to the planar triodes.

The grid pulse is flat to within ± 10 volts to maximize the EIA beam transmission and also to insure good intrapulse phase stability. Low cathode droop during the pulse is achieved with a depressed collection circuit in the high voltage interface. The high voltage interface also provides circuit grid pulse bypass, the EIA voltage and current divides, as well as heater power supply isolation.

The monitor and fault circuit detects excessive cathode voltages, average cathode current and average EIA body intercept current and sends a power interrupt command to

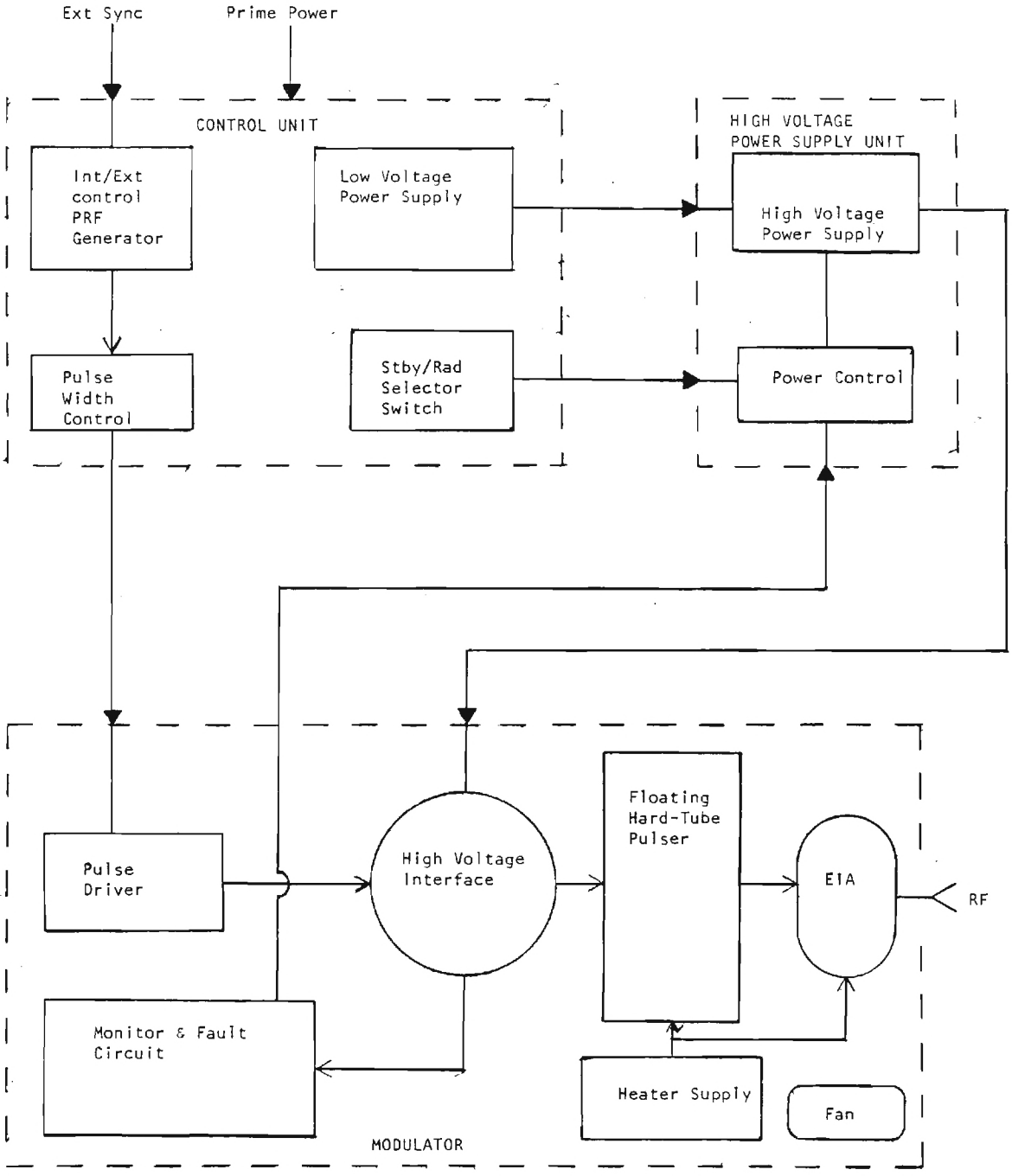

Figure 21. Simplified block diagram of the high voltage power supply/modulator.

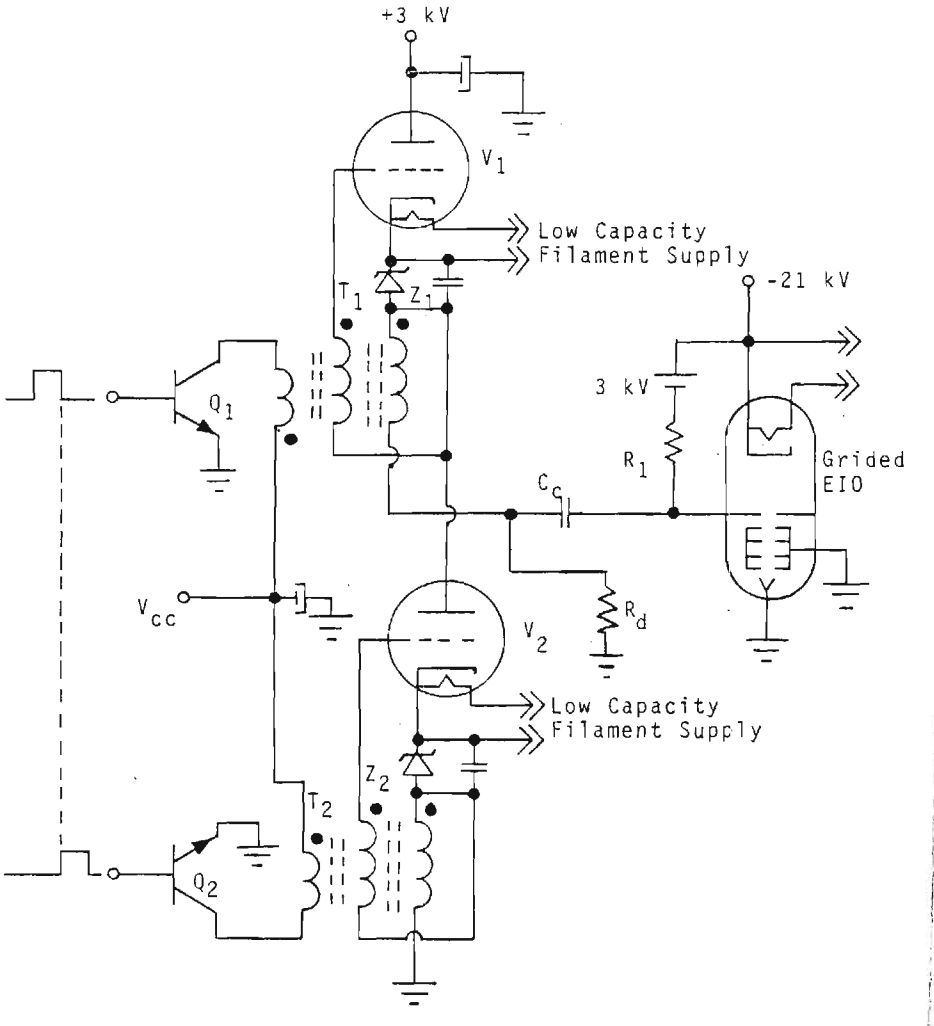

Figure 22. Hard tube - push pull pulser.

the HVPS. Due to the low energy storage design of the depressed collector circuit, a "crowbar" circuit is not required for pulse widths up to 1 μs.

3.4.3 RF PERFORMANCE

Table 10 lists the RF pulse specifications for the 95 GHz EIA transmitter RF output. These specifications represent values which can be easily verified and may not represent the ultimate performance of the transmitter. In particular, the figures for peak power, phase stability, bandwidth, and gain are based on measurements of two prototype tubes developed for the U.S. Army ERADCOM ET&T Laboratory. Figure 23 shows the power output versus frequency when the EIA is synchronously used at 95.0 GHz, while Figure 24 shows the power output versus frequency when the EIA is staggered tuned or bandwidth tuned.

TABLE 10. RF OUTPUT PULSE PERFORMANCE OF THE EIA

Frequency		94.0 to 96.0 GHz
Peak Power		2.0 kW
Duty		.01 maximum
Pulse Width		30 ns to 1 μs
PRF		1 kHz to 25 kHz
Rise and Fall Times 10% to 90%		20 ns maximum
Droop (power)		5% maximum
Ripple (power)		$\pm 2^{\%}$ maximum
Phase Stability		
Intrapulse		$\pm 2^{\circ}$ maximum
Pulse-to-Pulse		$\pm 5^{\circ}$ maximum
Gain (Typical, Saturated)		
@ 240 MHz, 3 dB Bandwidth	43 dB	
@ 400 MHz, 3 dB Bandwidth	31 dB	

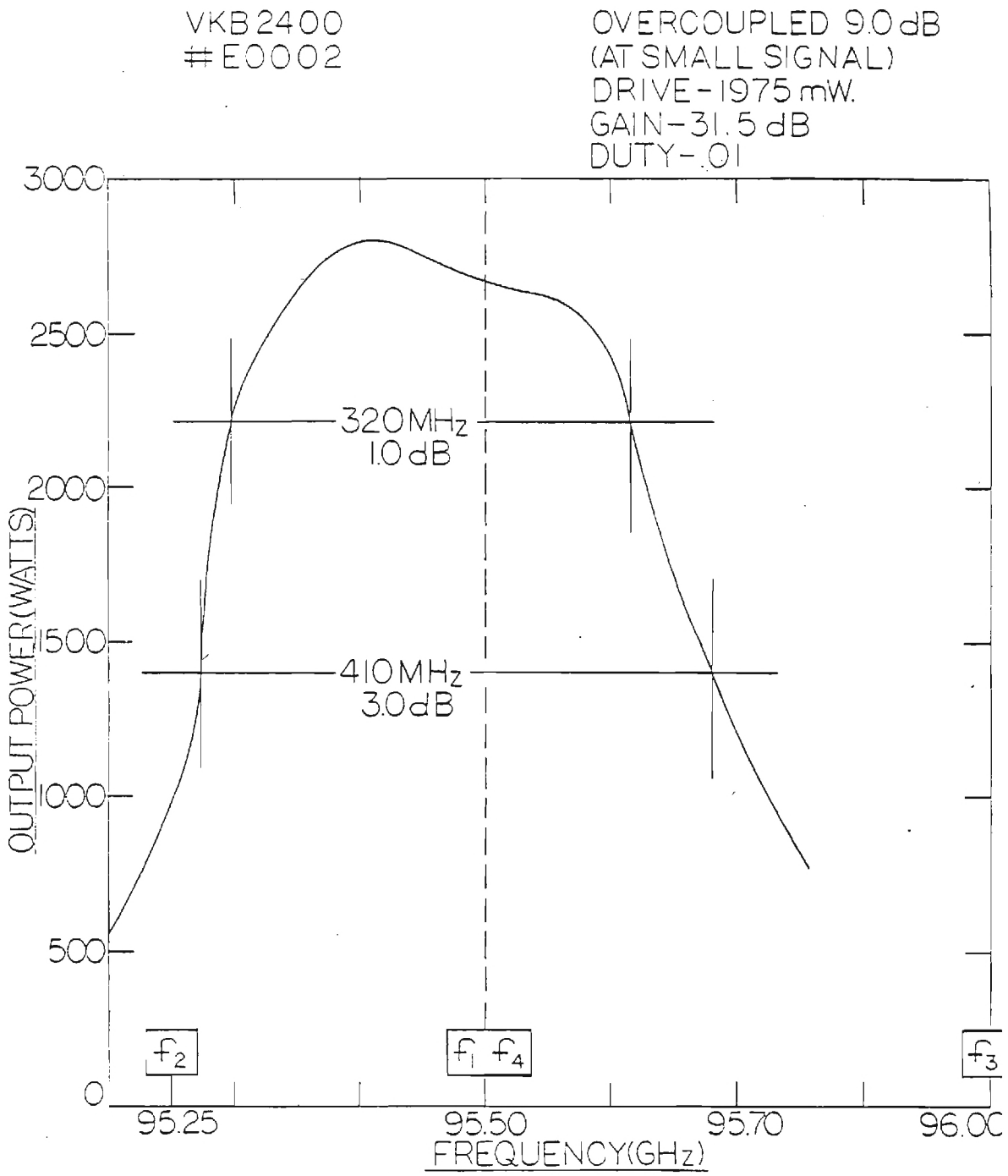

Figure 23. Power versus frequency (bandwidth tuned).

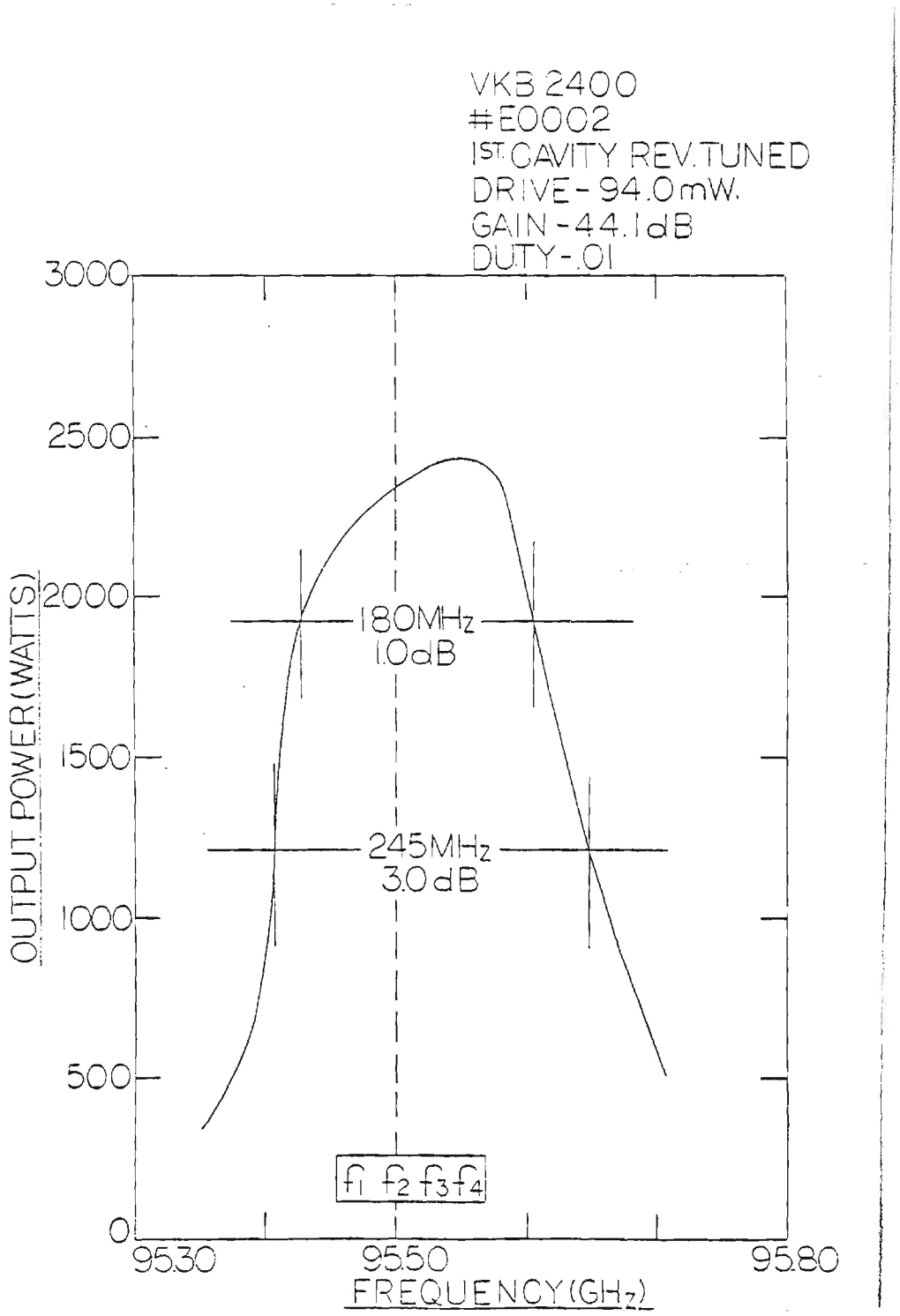

Figure 24. Power versus frequency (synchronously tuned).

SECTION 4
SYSTEM SENSITIVITY ANALYSIS

In this section, the final data on the 95 GHz radar parameters will be used to perform a sensitivity analysis of the expected system performance.

The radar sensitivity is derived using the radar equation in Section 1 which is repeated here for convenience.

$$RCS(min) = \frac{(S/N)(4\pi)^3 R^4 kTBFL}{P_T G_T G_R \lambda^2 N} \tag{44}$$

where:
- RCS (min) = minimum detectable radar cross section
- (S/N) = system signal to noise ratio
- R = slant range to the target
- k = Boltzmann's constant
- T = reference temperature
- B = receiver noise bandwidth
- F = receiver noise figure
- L = total losses
- P_T = peak transmitter power
- G_T = transmitter antenna gain
- G_R = receiver antenna gain
- λ = wavelength
- N = integration gain.

A tabulation of these parameters and the resulting minimum detectable RCS are given in Table 11. Pertinent parameters are discussed below.

4.1 RCS(min)

The minimum detectable RCS was specified at -60 dBsm desired and -50 dBsm required at a signal-to-noise ratio of 0 dB and 1170 meters slant range. The proposed design will achieve -67 dBsm for these conditions with a possibility of increased sensitivity.

TABLE 11. RADAR SENSITIVITY CALCULATIONS

Parameter	+ dB	- dB
S/N = 1	0	
$(4\pi)^3$	33	
R = 1170 m	122.7	
$kT = 4 \times 10^{-21}$ J		204
B = 4 MHz	66	
F = 7	7	
L = 10 dB	10	
P_T = 1 kW (2 kW)		30 (33)
$G_T = G_R = 44.5$		89
λ = 3.16 mm	50	
N = 2048		33
Totals	288.7	356 (359)

RCS_{min} or σ_{min} = -67.3 dBsm (-70.3 dBsm)

4.2 SIGNAL-TO-NOISE (S/N)

The signal-to-noise ratio was specified at 0 dB. Swerling [10] gives a lower bound on the measurement accuracy as a function of S/N ratio as follows:

$$\frac{\Delta_A}{A} - (2S/N)^{-1/2} \tag{50}$$

where Δ_A is the standard deviation of the measurement error, A is the amplitude, and S/N is the signal-to-noise ratio. The derivation assumes the amplitude being measured (A) is contaminated by Gaussian noise. When the S/N ratio is high enough for reliable

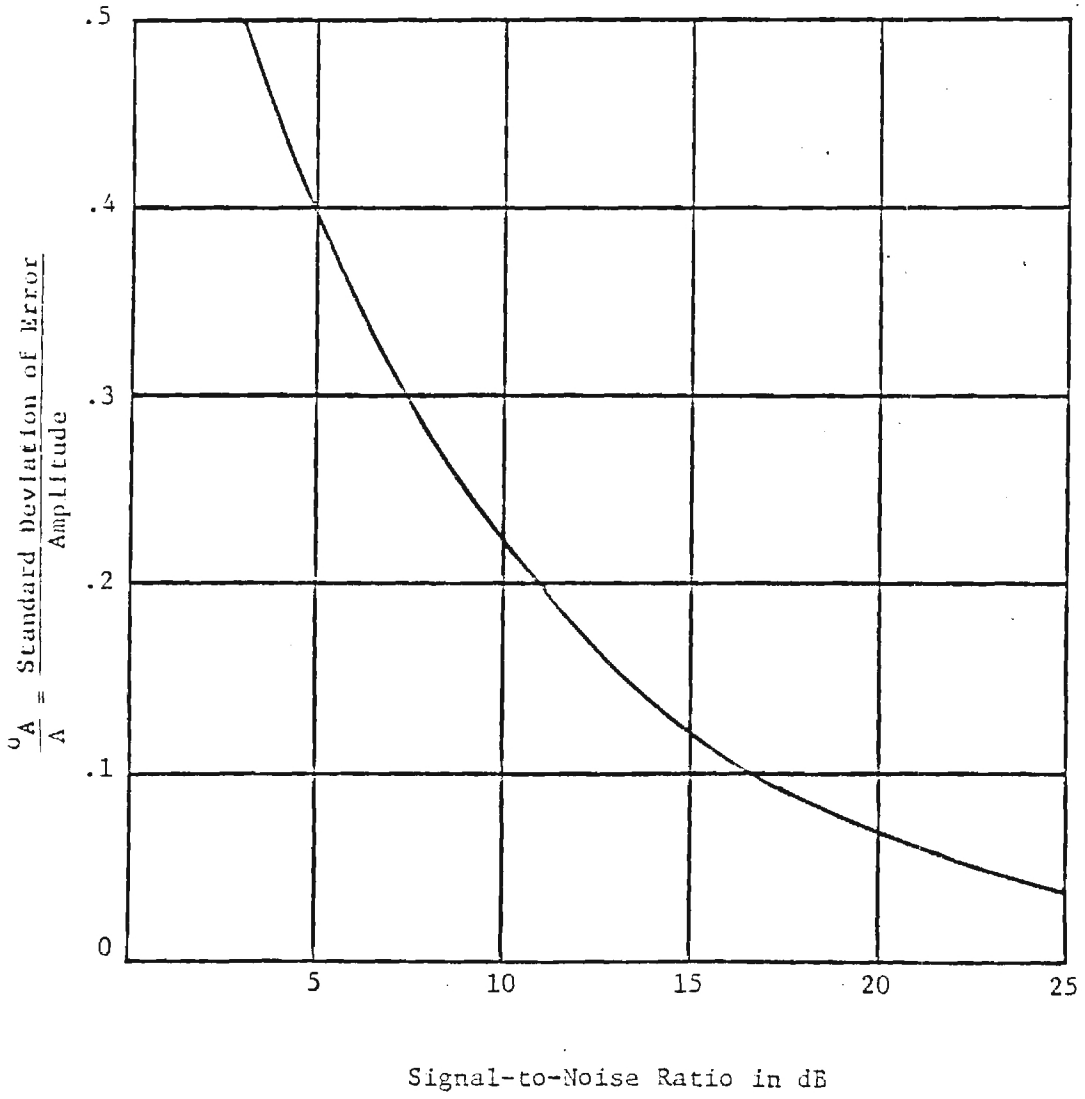

Figure 25. Standard deviation of measurement error vs. signal-to-noise ratio.

detection, the equality sign usually applies. Figure 25 is a plot of Equation 50. From the plot it is clear that for $\Delta_A/A \simeq 0.1$ (0.5 dB), a S/N ratio of 16 dB is required. Normally, a S/N ratio of 10 dB is specified (< 1 dB error) to provide a reasonable measurement accuracy. With these criteria, reliable measurements, corresponding to 10 dB S/N ratio, can be made of radar cross section down to -57 dBsm (-60 dBsm if P_T = 2 kW) with the proposed system.

4.3 RANGE

The slant range was determined by the range geometry. The RCS(min) of -67 dBsm corresponds to the maximum range of 1170 m. At the close in range of 504 m, an additional 15 dB of sensitivity is achieved.

4.4. RECEIVER SENSITIVITY (kTBF)

The receiver sensitivity is determined by the mixer/preamplifier single sideband noise figure and the effective noise bandwidth. Both of these have been maximized by selection of the IF frequency (500 MHz) and the use of narrow-band filtering (4 MHz). For a transmitted pulse width of 400 microseconds, the corresponding minimum bandwidth is 1.2/(400 μs) or 3 MHz. A wider bandwidth filter was selected to provide low phase distortion. To prevent phase distortion, the preliminary design required a 10 MHz filter for the proposed 200 μ s pulse, therefore, a decision was made to increase the pulse width with the resulting decrease in noise bandwidth and increase in sensitivity of 4 dB.

4.5 L - TOTAL LOSSES

The system losses are primarily due to losses through the switchable polarization assembly and the losses through the calibrator. Atmospheric losses at the ranges of interest are extremely small for clear weather, and it has been assumed that measurements will be restricted to "clear weather" days. The losses (in dB) are as follows:

Antenna Feeds	
Dual mode coupler (X2)	0.4
Transition (X2)	2.0
Waveguide switch (X2)	1.0
Waveguide (X2)	2.0

Calibrator	
Precision attenuators (X2)	2.0
Miscellaneous connections	2.0
Atmospheric	0.6
TOTAL	10.0 dB

4.6 P_T - PEAK POWER

The peak power is presently specified at a minimum of 1 kW. Past experiences have shown that peak powers of 2 kW are very probable. Therefore, an increase of 3 dB in sensitivity is possible, and is listed in the table in parentheses.

4.7 $G_T = G_R$ - ANTENNA GAIN

The requirements for antenna selection were covered in Section 2. If smaller targets (<20 m) are considered and/or a greater than 1 dB taper across the target is acceptable, larger antennas can be used and the sensitivity is increased. For example, if a 3 dB taper across the target is allowed, approximately 5 dB greater gain per antenna can be achieved with a resulting sensitivity of -77 dBsm.

4.8 N - INTEGRATION GAIN

For coherent integration/processing, the gain is ideally N, where N is the number of pulses coherently integrated. The limiting factors for the maximum gain achievable are the integration time (system data rate) and the maximum PRF of the transmitter. For the given range operations, the data rate is established at 10 Hz. For the PRF, the limiting factor is the EIA duty cycle which is less than 0.01. For a 400 ns pulse, the maximum PRF is 25 kHz and when combined with the data rate gives the maximum number of pulses that can be integrated as 2500. To simplify the processing, 2048 was selected with a PRF of 21 kHz (synchronous to the 1 kHz range clock). This gives a 33 dB integration gain for the above conditions.

Consideration was given to increasing the PRF to 50 kHz by reducing the pulse width to 200 ns. This would provide an additional 3 dB in integration gain, but would result in a loss in receiver sensitivity of 4 dB (increase in noise bandwidth from 4 to 10

MHz). Also, the high PRF increases the load on the processor. For these reasons, the 21 kHz PRF was selected.

4.9 CONCLUSIONS

Based on the above discussions, it is possible to improve the system sensitivity at some expense to other considerations (i.e., data rate, antenna gain taper). However, the bottom line is that an excess of 7 to 10 dB sensitivity above that desired can be achieved by combining state-of-the-art technologies (SS coherent sources, grid modulated EIA, EIA modulator development) with a novel coherent receiver/processor design. Based on this design, a system can be developed that is fully responsive to McDonnell range requirements.

SECTION 5
SYSTEM MAINTENANCE CONSIDERATIONS

This section will discuss the pertinent maintenance considerations for the proposed system. The proposed system, as will other current millimeter wave systems, will contain a number of components which will work improperly or fail if the environmental operating conditions vary significantly from laboratory conditions. In particular, it will be necessary to heat the system in winter and cool it in summer conditions. Also, it will be extremely important to keep the system dry and dust free. In any outdoor environment, this requires that filtered, conditioned air (either heated or cooled) be forced over the components to ensure reliable operation.

The primary items which may require replacement in periodic manner are in the high power coherent transmitter stage. The extended interaction amplifier (EIA) tube is guaranteed for 1,000 hours although limited testing (of three tubes) has yielded a 5,000 hour average life. The planar triodes which drive the high voltage transformer in the modulator also have a limited life of 1,000 hours (warrantee). Other high voltage modulator components should have a much longer life, but could fail eventually.

The solid state driver as a system has been guaranteed for 100,000 hours by Hughes Aircraft. However, experience has shown that often failures may occur during the first few hours of operation of such components. Once these components are "burned in" they become extremely reliable.

The system electronic components should be as reliable as any standard piece of laboratory equipment and should not require maintenance. Since the signal processor is digital, drifts and other electronic problems should be greatly reduced. The digital and analog components will probably have an early failure problem similar to that expected for the solid state driver, so it is recommended that a suitable spare parts kit be maintained on-site with the radar.

SECTION 6
CONCLUSIONS AND RECOMMENDATIONS

Based on the results of this study to design a 95 GHz measurements radar for the Grey Butte test range, the following conclusions can be drawn:

1. Three systems are feasible using different technologies. These include an incoherent EIO system, a solid state coherent system, and a coherent EIA system.
2. The EIO and solid state coherent systems will yield minimum radar cross-section sensitivities of -50 dBsm for a signal-to-noise ratio of 1. While the EIA system will yield a sensitivity of -67 dBsm.
3. The estimated cost of the EIA system is 25% greater than the EIO or solid state systems.
4. After a decision by McDonnell on the preferred approach, a more detailed design was performed on the EIA system, and it was determined that the desired sensitivity and dynamic range requirements could be met by the system.
5. The estimated cost for the system was approximately $720,000 based on a 15-month program which would start in April of 1982.
6. The maximum allowable antenna size to achieve a 1 dB taper on a 30-foot target results in a 2^{o} by 0.5^{o} beam.
7. Specular multipath may cause variations in the target illumination as well as calibration errors.
8. The use of the system in a "ground plane enhancement" mode is not feasible because this would require reducing the antenna size with a corresponding reduction in antenna gain.
9. The target support structure is expected to have a radar cross section of -40 to -50 dBsm.
10. The atmospheric effects of the system will be appreciable during rain or heavy dust conditions. The effect will be to reduce the system sensitivity 10 dB or more as well as effect the calibration and target returns.

A number of recommendations follow from the above conclusions, including:

1. Development of the system should begin as soon as feasible to avoid additional inflationary cost increases.
2. Two fan beam antennas are recommended (0.5^{o} by 2^{o}) to provide full target illumination as well as high antenna gain.
3. Measurements should be performed on the RCS of the support structure at 95 GHz.
4. Provisions should be made to provide conditioned air for the system when mounted on the tower at the Grey Butte Test Range.
5. Measurements should be suspended during rain or heavy dust conditions.
6. Large targets should always be placed on the far target support to avoid illumination and near field problems.

SECTION 7
ESTIMATED SYSTEM COST

THIS DOCUMENT HAS NOT RECEIVED FINAL REVIEW OR APPROVAL BY GEORGIA TECH'S MANAGEMENT AND SHOULD, THEREFORE, BE CONSIDERED ONLY AS INFORMATION TO PERMIT YOUR ORGANIZATION TO DETERMINE WHETHER A BASIS EXISTS FOR FURTHER DISCUSSION. THE GEORGIA INSTITUTE OF TECHNOLOGY OFFICE OF CONTRACT ADMINISTRATION (404/894-4817) IS THE ONLY OFFICE AUTHORIZED TO SUBMIT OFFICIAL PROPOSALS AND NEGOTIATE R&D GRANTS AND CONTRACTS.

This section will present a cost estimate for the 95 GHz Measurement Radar System based on current estimates of manpower and materials costs. It should be noted that these estimates should in no manner be considered a binding proposal but are presented here for planning purposes only. This estimate assumes that Georgia Tech would provide the system design, would construct the high power EIA transmitter stage, would develop the signal processor, and would provide system checkout, documentation, and training. The Extended Interaction Amplifier tube would be purchased from Varian Canada, and the coherent source/receiver would be developed under a subcontract to Hughes Aircraft Corporation. The manpower rates used in the estimate assume current Georgia Tech Research Institute rates plus a 10 percent "inflation factor" for that portion of work performed after July 1, 1982. It is assumed that work would begin in March 1982 and last 15 months.

Table 12 gives the estimated required manpower for each of the tasks that must be performed in terms of man months of a given catagory. A total of approximately 75 man months of effort would be required for this effort. Table 13 gives an estimate of the materials cost and includes the subcontract to Hughes Aircraft Corporation ($100,700). These costs total approximately $219,000. Table 14 summarizes the total estimated costs including manpower, materials, travel, benefits, and overhead. The total estimated cost is thus approximately $720,000. Table 15 gives a schedule for the development effort assuming a 15 month total program. The effort would consist of system design, coherent driver/receiver development, EIA procurement, modulator development, signal

processor development, system fabrication, system test, on site training, and documentation. Note that any delays in the start date or extension in program length would more likely result in the incurring of additional costs due to inflation factors.

TABLE 12. SYSTEM COMPONENT AND MATERIALS COSTS

SUBSYSTEM	ESTIMATED COST ($)
SS Coherent Driver/Receiver	100,700*
HVPS/Modulator	7,500
Extended Interaction Amplifier	75,000
Antennas	5,000
Dual Mode Couplers	4,100
WG Switch/Termination	7,240
Signal Processor	6,200
Calibrator	6,000
System Assembly/Misc WG	7,000
Total	$218,740

*Subcontract to Hughes Aircraft Company.

TABLE 13. SYSTEM MANPOWER REQUIREMENTS (MM)

TASK	SENIOR ENG	JUNIOR ENG	TECH/MECH	SEC
System Design	7	0	0	0
Signal Processor	2	2	2	0
Calibrator	1	1	1	0
TCE	2	2	2	0
Control Panel	0	1	1	0
Power Supplies	0	1	.5	0
HVPS/Modulator	4	3	2	0
RF/System Assembly	4	3	4	0
System Test	7	0	3	0
Training	1	1	0	0
Documentation	1	3	1	1
Program Management	10	1	0	2
Totals	39	18	16.5	3

THIS DOCUMENT IS NOT AN OFFICIAL PROPOSAL

TABLE 14. TOTAL ESTIMATED COST

COST ITEM	AMOUNT ($)
Direct Manpower Costs*	238,750
Components and Material	118,040
Subcontract to HAC	100,700
Travel	13,000
Employee Benefits	27,700
Total Direct Costs	498,190
Overhead (0.55 of MTDC)	221,370
Total Estimated Cost	719,560

*Labor rates are based on an anticipated 10% increase in average salaries beginning July 1, 1982 with program completion in June, 1983.

TABLE 15. PROGRAM SCHEDULE

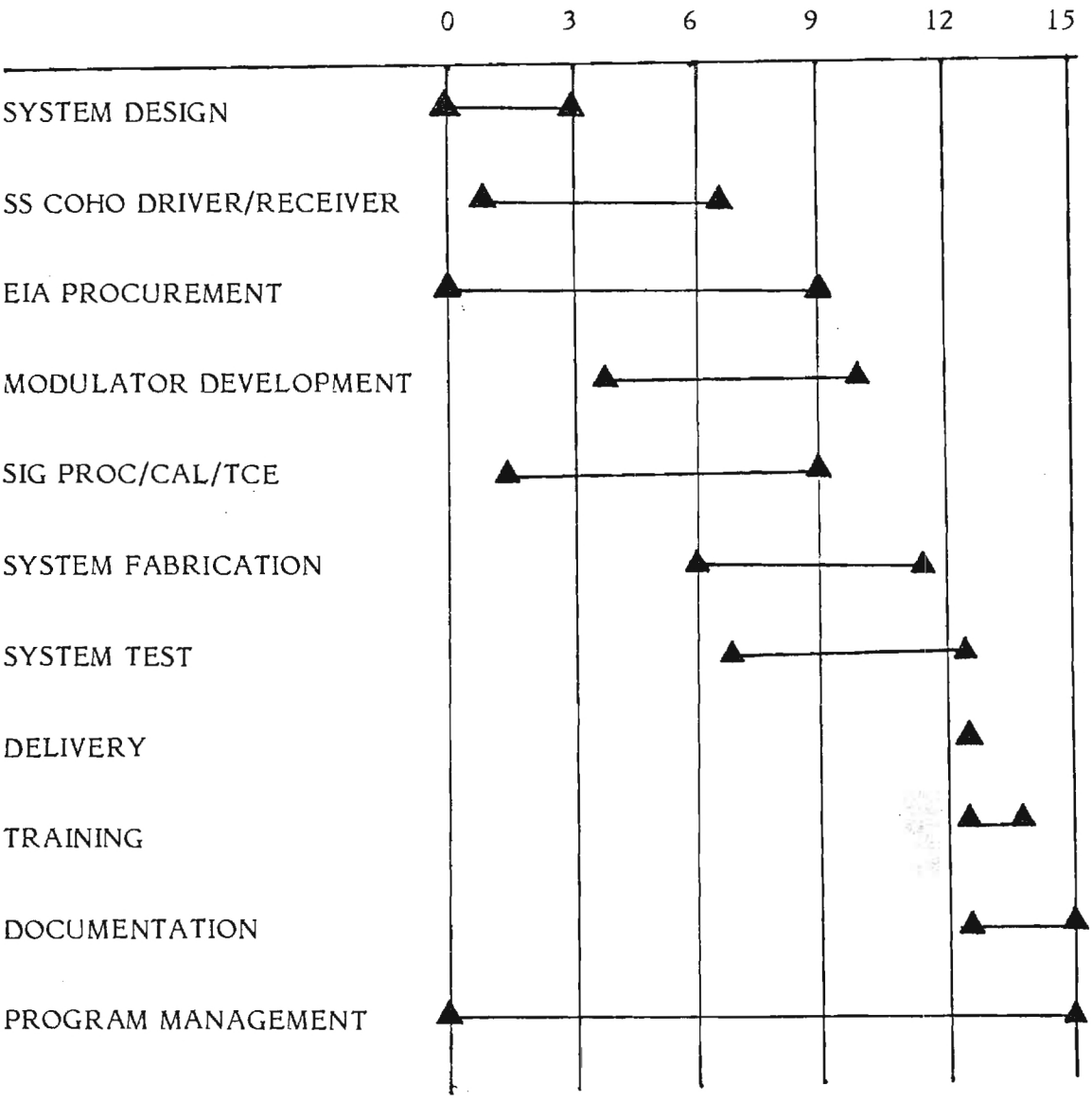

References

1. N. C. Currie, "Progress Report No. 1 on Purchase Order F13549," Monthly Progress Report on Purchase Order F13549, Georgia Institute of Technology, Atlanta, Georgia, October 1981.

2. John D. Kraus, Antenna, McGraw-Hill Book Company, 1950.

3. David K. Barton, "Low-Angle Radar Tracking," Proceedings of the IEEE, Vol. 62, June 1974, pp. 687-704.

4. Simon Ramo and John R. Whinnery, Fields and Waves in Modern Radio, Wiley and Sons, London, (Second Edition), 1960, pp. 199-307.

5. N. C. Currie, et al, "Analysis of the Radar Return From Rain at Frequencies of 9.375, 35, 70, and 95 GHz," Technical Report No. 2 on Contract DAAA25-730C-0256, Georgia Institute of Technology, Atalnta, Georgia, February 1975, ADD007254.

6. "Rain Attenuation Measurements at 94 GHz: Comparison of Theory and Experiment," AGARD Millimeter and Submillimeter Wave Propagation and Circuits Conference, Munich, Germany, September 1978.

7. E. E. Martin, "Radar Reflectivity of Dust Cloud Lofted by MISERS BLUFF II High Explosive Test," Final Technical Report on Contract DNA001-77-C-0269, Georgia Institute of Technology, Atalnta, Georgia, March 1979.

8. "Operation and Maintenance Manual for 44476H-1001 94 GHz Coherent Instrumentation Front End," Hughes Internal Report, October 1980.

9. "Solid State Millimeter Wave Products Catalog," Hughes Aircraft Corporation, Subsystems Issue, Model 42266H-2000, 94 GHz Coherent Instrumentation Radar Front End.

10. M. I. Skolnik, ed., Radar Handbook, McGraw Hill, New York, 1970, p. 47.